THROUGH ASPHALT DETECTION OF CORROSION DAMAGE IN CONCRETE USING GROUND-COUPLED GPR

by

Tye Minion

Submitted in partial fulfilment of the requirements
for the degree of Master of Applied Science

at

Dalhousie University
Halifax, Nova Scotia
July 2014

Table of Contents

List of Tables

List of Figures

Abstract

Many transportation departments (DOT) use Bridge Management Systems (BMS) to assist in planning, maintenance and repairs. BMS keep track of a number of aspects regarding a department's bridge infrastructure that include location, data of construction, "original" drawings, and current state of the structure in addition to many other parameters. The most important of these is the current condition. This is generally assessed using visual inspection techniques. These inspection techniques are very subjective and lead to high contingencies for DOT's and conservative bids from contractors. To assist in developing more accurate condition assessment of bridge deck deterioration, this thesis examines a number of methods that use a Ground Penetrating Radar (GPR) system with a single Ground Coupled Antenna (GCA) on bridge decks with an asphalt overlaid deck.

Currently, when assessing bridge deck slabs with an asphalt overlay using GPR, air coupled antennas need to be used in order to determine the permittivity of the asphalt. If the permittivity of the asphalt is known then the permittivity of concrete can be determined using the reflection coefficient and then the losses due to geometric spreading can be calculated. A number of laboratory tests were conducted using asphalt and concrete samples to investigate the feasibility of determining the permittivity of the uppermost layer using a ground coupled antenna. Once the permittivity of the laboratory samples was accurately determined, field tests were conducted. The field testing consisted of assessing the conductivity of concrete for four unpaved bridge decks in Nova Scotia. The conductivity results were compared with a method being developed by another graduate student in the same research team. The field tests strongly indicated that the surface reflection for a GCA is unable to be used to accurately determine the permittivity of concrete. However one of the structures had a number of asphalt patches that produced reasonable permittivity and conductivity results.

Field tests to confirm the accuracy of the method in determining the permittivity of asphalt using a GCA were unable to be done due to the lack of available test subjects; for this reason it was assumed from the laboratory results that a GCA is able to accurately determine the permittivity of asphalt. A number of methods were proposed for analysing bridges with an asphalt overlay; but due to the lack of ground truth data and limited sample size, success was assumed to be achieved if the estimated permittivity and conductivity value were within the generally accepted range. The two proposed methods tested were, a conductive model that assumed a constant signal velocity in concrete and a semi-conductive model that assumed the asphalt was non-conductive. The results from these tests indicated that asphalt may be treated as a non-conductive medium. The tests also raise the question of whether the asphalt/concrete interface reflection can be used to accurately determine the permittivity of concrete.

List of Abbreviations and Symbols Used

AU Amplitude Units

BMS Bridge Management System

DOT Department of Transportation

GCA Ground Coupled Antenna

GPR Ground Penetrating Radar

NDT Non-Destructive Testing

SHE Standard Hydrogen Electrode

T-R Transmitter Receiver

TWTT Two Way Travel Time (ns)

VI Visual Inspection

A_{air} Amplitude of electromagnetic wave when antenna is held in the air, direct wave (AU)

A_{bar} Amplitude of electromagnetic wave after reflecting from rebar (AU)

A_{bttm} Amplitude of electromagnetic wave after reflection from bottom of deck (AU)

A_i Amplitude of electromagnetic wave i (AU)

A_m Amplitude of electromagnetic wave interface reflection (AU)

A_o Amplitude of emitted electromagnetic wave (AU)

A_r Amplitude of the reference electromagnetic wave (AU)

$A_{wave\ 2'}$ Amplitude of electromagnetic wave surface reflection just prior to reflection (AU)

$A_{wave\ 2}$ Amplitude of electromagnetic wave surface reflection just after reflection (AU)

B Magnetic Field (Tesla, T)

B_o Initial Magnetic Field (Tesla, T)

c Speed of light in a vacuum (300 mm/ns)

d Distance between the transmitter and receiver (mm)

d_i Distance the electromagnetic wave travels in i^{th} layer (mm)

E Electric Field (Newtons/Coulomb, N/C)

E_o Initial Electric Field (N/C)

h_i Height of layer i (mm)

J Current Density (A/m^2)

j Imaginary number

r Reflection coefficient

t Time (ns)

v_i Velocity of electromagnetic wave in i^{th} layer (mm/ns)

x_r Distance of reference electromagnetic wave from source (mm)

x_i Distance of electromagnetic wave from source (mm)

z Distance along the wave (mm)

α_i Attenuation of i^{th} layer (Np/mm)

β Phase constant (rad/m)

ε	Complex permittivity (F/mm)
ε'	Real component of permittivity (F/mm)
ε''	Imaginary component of permittivity (F/mm)
ε_r	Relative permittivity
ε_o	Permittivity of free space (F/mm)
θ_i	Angle of incidence (Degrees)
θ_t	Angle of transmission (Degrees)
μ	Magnetic permeability (H/m)
μ_r	Relative Magnetic permeability
μ_o	Magnetic permeability of free space (H/m)
ρ	Charge density
σ	Conductivity (S/m)
τ_{ij}	Transmission coefficient from layer i to j
ϕ	Correction factor when using the air wave as the reference wave
ω	Angular frequency (rad/s)

Acknowledgments

I would like to thank my supervisors, Dr. Barnes and Dr. Newhook, for their assistance and guidance. I would also like to acknowledge Adam Sketchley for his important role in the success of this thesis through the discussions of ideas and collaboration.

I would also like to thank Ted McPeak and Darly Hurts with T.D.M. Engineering Ltd. for their assistance and constant support during field and laboratory testing in Alberta. I would also like to acknowledge Alberta Transportation for allowing me to conduct my field tests in Alberta.

I would also like to thank Nova Scotia Transportation and Infrastructure Renewal for allowing there bridges to be tested and Eileen McEwen for collecting the data that was using in the single layer analysis.

Finally I would like to thank the National Science and Engineering Research Council of Canada for their financial support.

Chapter 1 Introduction

Bridge Management Systems (BMS) are employed by many transportation departments. These management systems are essentially databases that are used to keep a record of the bridges under the control of the department. The BMS keeps track of many parameters including the type of structure, location, age, past work performed on the structure, and current structural condition among others. This information is then used to assist in planning, maintenance schedules and budgets. The ability of a BMS to perform its intended function effectively is based on the quality of the input information. Type of structure, location, age and past work are easy to keep track of and are fairly accurate due to the nature of the information. It is more difficult however to obtain accurate information regarding the current state of the structure.

For steel reinforced concrete bridges, one of the most concerning areas is structural deficiencies due to corrosion of the steel reinforcement in the bridge superstructure. Corrosion can be caused by chloride which comes from deicing salt that is used to prevent the formation of ice on bridge decks during the winter in cold climates. Over time the deicing salt will diffuse into the asphalt and concrete through interconnected pores and eventually reaching the rebar. Once the concentration of salt at the rebar has reached a critical level, corrosion will occur.

A number of non-destructive testing (NDT) techniques are available to help quantify the damage caused by corrosion that can be used as inputs to a BMS. These techniques include: visual inspection (VI), chain dragging, half cell measurements, impact echo, infrared thermography, and ground penetrating radar (GPR).

Visual inspection and chain dragging are the two most commonly used NDT techniques due to their relatively low cost. Visual inspection is also a relatively fast inspection technique that is used to provide conditional assessment on most of the major bridge components. One of the benefits of VI is that it can often be done at the same time as other inspection techniques. VI is not recommended for detecting corrosion of asphalt

overlaid bridge decks (Sohanghpurwala, 2006). The asphalt inhibits propagation of concrete damage resulting it minimal visual evidence of damage in the asphalt. Even though VI is subjective and its accuracy is variable it is often used for bid quantities in tenders.

Manual sounding or chain drag is a slower method that is commonly used to detect delamination for most of the main structural elements. Delamination occurs because as rebar corrodes the cathodic area expands causing the concrete to crack. When a chain is dragged or a hammer is struck against the cracked concrete a "hollow" sound is created. This technique is relatively inexpensive and requires minimal skill from the operator. However, it is also subjective, requiring the interpretation of the operator to detect defects, and susceptible to error caused by debris on the surface and ambient noise. Chain dragging is often used to map areas requiring repair on the decks during rehabilitation and hammers are used on most other surfaces. The damaged areas are outlined with paint and a tape measure is used to determine total delaminated area. This method is unable to be used on asphalt overlaid bridge decks because it will detect debonding between the asphalt and concrete in addition to delamination between the concrete and rebar (Alberta Transportation, 2007). Asphalt also insulates the sound waves making it difficult to hear and therefore detect delaminations.

Half cell or reference electrode measurements is an inspection technique that is used to determine the potential for corrosion to occur. This technique determines the probability of corrosion by detecting the electric potential difference between the concrete and reference electrode. The accuracy is affected by several parameters including the moisture content of the concrete and the concrete cover. It is relatively labour intensive and requires lane closures. Half cell measurements provide spatial maps of corrosion potential of the entire deck which are used to determine the current state of the structure and which can be entered into the BMS. This technique is ultimately used to help determine which structures require repair. Half cell testing is not

recommended for deck with asphalt overlays (Sohanghpurwala, 2006). According to ASTM C876 cell can only be used on bare concrete decks.

Ground Penetrating Radar (GPR) is a NDT method that uses electromagnetic pulses to detect discontinuity in permittivity. GPR has shown promise and can spatially map the damage of a deck through the use of grids and a survey wheel. GPR testing has the potential to be conducted without lane closures. It does require a skilled operator and is more expensive than the other techniques. GPR emits an electromagnetic (EM) wave and records the time it takes for the wave to reach the receiver and the amplitude of the returning wave. One of the earliest techniques investigated variations in the amplitude of the asphalt concrete interface reflection as an indicator of deterioration (Holt, 1982). This method had limited success because amplitude varies for a number of different reasons. Later research, which mathematically adjusted the raw data, had success in using the asphalt concrete interface reflection to detect deteriorated areas (Maser, 1991; Alongi at. el., 1992). It was noticed that variations in rebar amplitude were more effective in detecting areas of deterioration because the signal weakens due to the presents of chloride (Alongi at. el., 1992).The issue with Alongi's method is that variations in rebar amplitude can be due to geometric spreading, depth, in addition to chloride, attenuation. Recent research has looked into removing the effects of geometric spreading, leaving attenuation as the main cause of rebar amplitude variation and has resulted in 3% error when estimating the deteriorated area (Barnes at el., 2008). Up to now these methods indicate whether an area is likely damaged or not at a specific moment in time. The next step in this research is to determine the level of damage using a variable with physical meaning. The variable chosen to assess the level of damage is conductivity. Conductivity causes attenuation and is related to the chloride content of concrete (Alongi at. el., 1992).

This thesis will focus on determining the conductivity of concrete for bridges with an asphalt overlay, which will be referred to as multilayer systems; bridges without an asphalt overlay will be referred to as single layer systems.

The papers referenced above all used air coupled GPR antenna because air coupled antennas can be used to determine the permittivity of the top layer. There are a number of issues with air coupled antennas, with low resolution being the main one for bridge decks. The resolution is so low individual rebar cannot be identified. To increase resolution a ground-coupled antenna (GCA) will be used. GCA increase the resolution because they have a smaller radar footprint at the rebar due to their closer proximity to the rebar. The radar footprint is the area that the returning signal is effected by, as the EM wave becomes farther from the source the footprint becomes larger. The increase in resolution provided by GCA's allows smaller areas of damage to be detected providing a more accurate estimate of repair area. GCA have not be used a lot for bridge surveying because they cannot determine the permittivity of the top layer due to wave interference, which will be discuss in subsequent sections.

The goal of this thesis is to determine the conductivity of concrete using a GCA on concrete bridges with an asphalt overlay. In order to reach this goal a number of specific objectives have been set which are:

1. Determining the appropriate geometric spreading model of the antenna;
2. The effects of asphalt and concrete on the direct couple of a GCA;
3. The conductive nature of asphalt with respect to electromagnetic theory; and
4. A model for determining the conductivity of concrete on asphalt overlaid bridge decks.

Chapter 2 Corrosion

Refined metals are unstable at atmospheric conditions, with a few exceptions, and corrosion allows refined metals to revert to their natural and "stable" state (Schwietzer, 2009). This means corrosion is the "default" process for refined metals and will occur unless something inhibits it. When steel rebar is embedded in concrete this process is prevented by the formation and maintenance of a passive layer that is stable due to the high pH of concrete, which is generally in the range of 12-13 (Broomfield, 2006).

There are a number of conditions that can cause the passive layer on the rebar to be overcome including bacteria, stray electric current, carbonation, and chloride penetration (Broomfield, 2006). Bacteria and stray electric current are uncommon in bridge structures and will therefore not be discussed. Carbonation and chloride will be discussed.

2.1 Half Reaction

Corrosion is a series of electrochemical reactions that converts solid iron into iron ions while converting water and oxygen into hydroxide. The iron half reaction, Equation 2-1, is the anodic or oxidation reaction where electrons are lost. The oxygen water half reaction, Equation 2-2, is the cathodic or reduction reaction where electrons are gained (Callister & Rethwisch, 2012). These two reactions must maintain electric neutrality which means the same number of electrons must be lost in the anodic reaction as gained in the cathodic reaction.

$$2\mathrm{Fe} \rightarrow\ 2\mathrm{Fe}^{2+} + 4\mathrm{e}^{-} \qquad \textbf{2-1}$$

$$\mathrm{O}_2 + 2\mathrm{H}_2\mathrm{O} + 4\mathrm{e}^{-} \rightarrow 4\mathrm{OH}^{-} \qquad \textbf{2-2}$$

These two reactions ideally produce an electric potential of -0.440 V and 0.401 V for Equations 2-1 and 2-2, respectively, resulting in a total electric potential of 0.841 V (Callister & Rethwisch, 2012). In order for corrosion to occur the electric potential must

be positive, otherwise the reaction will be reversed. It should be noted the electric potential quoted above is achieved under very idealized and controlled conditions and in reality the electric potential will be different. The difference in laboratory testing and the field can be accounted for by different electrode composition as well as difference electrolyte solutions and concentrations among others.

The reactions presented by Equations 2-1 and 2-2 will occur provided they produce the highest electric potential in their system. If a zinc anode were added to the system described by Equations 2-1 and 2-2 the iron half reaction, Equation 2-1, would be replace with the reaction presented in Equation 2-3. The electric potential of Equation 2-3 is -0.763 V, resulting in a total electric potential of 1.164 V which is a higher electric potential than 0.841 V. The fact that the zinc will corrode before iron has been used to protect steel from corrosion through the use of sacrificial zinc anodes.

$$\mathrm{Zn} \rightarrow \mathrm{Zn}^{2+} + 2\mathrm{e}^{-} \qquad \textbf{2-3}$$

For any half reaction to occur a number of conditions must be met. First the anode and cathode must be electrically connected. In standard diagrams, Figure 2-1, this is shown with a wire. In reinforced concrete systems this electrical connection is provided by the interconnected rebar grid. The second condition is that the anode and cathode must be in an electrolyte that allows the movement of ions between the electrodes. This is often represented through the use of a “salt bridge” or the anode and cathode are immersed within the same electrolyte. For concrete systems the anode and cathode are in the “same” electrolyte. The reason that “same” is in quotations because the exact make up and concentration of the electrolyte in concrete may vary along the length of the bar.

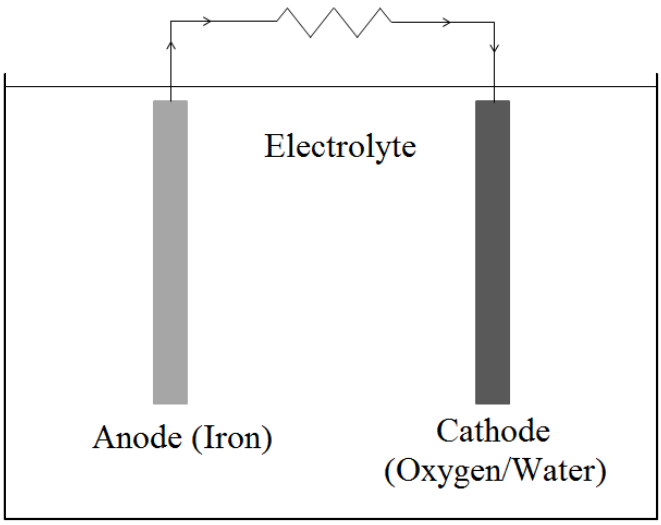

Figure 2-1: An idealized corrosion cell

2.2 Formation of Corrosion Products

The formation of "rust" occurs when the products of the half reactions described in Equations 2-1 and 2-2 react to produce hydrated ferric oxide or rust through a series of reactions. This series of reactions are described using Equations 2-4, 2-5, and 2-6 (Broomfield, 2006).

$$Fe^{2+} + 2OH^{-} \rightarrow Fe(OH)_2 \qquad \textbf{2-4}$$

$$4Fe(OH)_2 + O_2 + 2H_2O \rightarrow 4Fe(OH)_3 \qquad \textbf{2-5}$$

$$2Fe(OH)_3 \rightarrow Fe_2O_3 \cdot H_2O + 2H_2O \qquad \textbf{2-6}$$

As the reaction progresses the volume taken up by the products increases. Ferrous hydroxide occupies a volume 4 times that of the iron used to form the ferrous hydroxide. Ferric hydroxide occupies 4.5 the volume and hydrated ferric oxide increases the volume up to 7 times that of iron (Mansfield, 1981). This increase in volume causes tensile stresses to develop in the concrete resulting in cracks and delaminations. As the concrete delaminates and cracks, salt and water are able to enter the concrete more

easily through the cracks. The increase of salt and water near the rebar causes more severe corrosion at a faster rate than before cracking.

In certain cases there is a low amount of oxygen at the anode causing the iron to stay in solution preventing the formation of rust (Page and Page, 2007). This type of corrosion is called black or green rust and most commonly occurs under water or waterproof membranes (Broomfield, 2006). Since black corrosion does not cause cracking it is very difficult to detect using visual inspection or chain dragging.

2.3 Electrical Chemistry

The electric potential obtained from standard oxidation reduction potential charts is produced under idealized and highly controlled laboratory conditions (Callister & Rethwisch, 2012). The actual electric potential produced in the field is affected by a number of factors that include the concentration of the electrolyte, temperature and even pressure (Mortimer, 2000). The electric potential is important because it will determine whether corrosion occurs. A simplified Pourbaix diagram, Figure 2-2, shows the relationship between the pH, electric potential, where SHE is Standard Hydrogen Electrode, and state of corrosion. The diagram presents three possible states of corrosion: immunity, passivation, and corrosion. When iron is in a state of immunity it will not allow the dissolution of iron ions. The passive state is when the iron ions form but will react to produce a passive layer, Fe_2O_3 and Fe_3O_4, that will prevent further corrosion. Finally corrosion is when iron ions are formed and they react to produce rust.

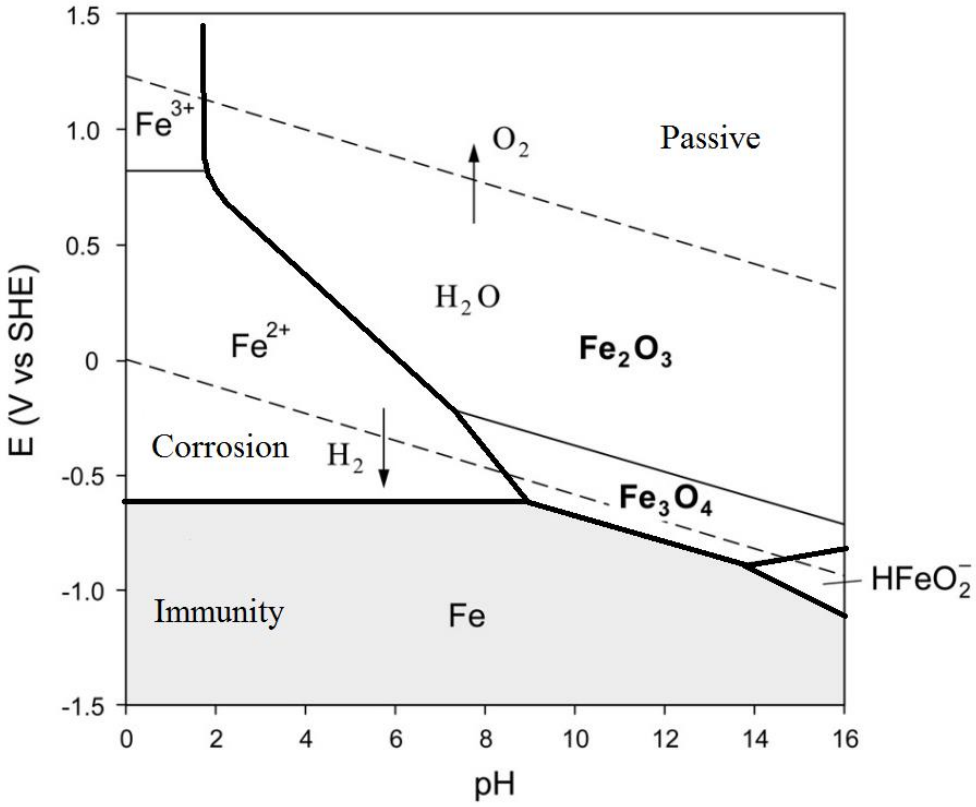

Figure 2-2: Simplified Pourbaix diagram showing corrosion states (Angst, 2011)

The pH of the concrete pore water solution is naturally high, 11 to 13. This is high enough that the steel is in the passive state. The layer of iron oxide produced in the passive state reduces the rate of iron dissolution (Page and Page, 2007). If corrosion is to occur either the pH must drop as in the case of carbonation or chloride must be present to overcome the passive layer (Page and Page, 2007).

Carbonation is when carbon dioxide dissolves in water, forming carbonic acid as seen in Equation 2-7. The carbonic acid reacts with the calcium hydroxide that is in the pore solution to from calcium carbonate and water, as per Equation 2-8 (Broomfield, 2006). Concrete generally has such a high amount of calcium hydroxide that not all of it is dissolved in the pore solution which results in the pH remaining constant at first (Broomfield, 2006). Over time the amount of calcium hydroxide will decrease resulting in a drop in pH which will cause a shift from the passive state to the corrosion state.

$$CO_2 + H_2O \rightarrow H_2CO_3 \quad \textbf{2-7}$$

$$H_2CO_3 + Ca(OH)_2 \rightarrow CaCO_3 + H_2O \quad \textbf{2-8}$$

Carbonation occurs in porous concrete which is common when the concrete has a high water cement ratio (Broomfield, 2006). The process is rare in modern bridge structure because low water cement ratios are often used (Broomfield, 2006), helping to ensure that a low volume of interconnected permeable voids is provided. Carbonation is not detectable with GPR but it can affect the chloride threshold value (Glass et al., 1991).

Chloride on bridge decks commonly comes from deicing salts. The chloride enters and travels through the interconnected pores in the concrete. Once the chloride reaches the rebar at high enough concentrations corrosion will occur. Corrosion due to chloride is complicated and the exact mechanics of the process are not well understood (Silva, 2013). What is known about chloride induced corrosion is that it can occur at high pH levels (Page and Page, 2007) and the chloride ions act as a catalyst which reacts with the iron ions (Broomfield, 2006) as seen in Equations 2-9 and 2-10. Even though the chloride ions are not used up in the reaction there needs to be a certain concentration before the steel depassifies (Page and Page, 2007). This concentration is referred to as the chloride threshold and representing the threshold as the ratio of chloride ion concentration to hydroxide concentration a ratio of 0.6 is required for depassification. A ratio of 0.6 is approximately 0.2 % chloride by weight of cement if the chloride diffused into the concrete (Broomfield, 2006).

$$Fe^{2+} + 2Cl^- \rightarrow FeCl_2 \quad \textbf{2-9}$$

$$FeCl_2 + 2OH^- \rightarrow Fe(OH)_2 + 2Cl^- \quad \textbf{2-10}$$

$$Cl^- + H^+ \rightarrow HCl \quad \textbf{2-11}$$

Chapter 3 Testing Methods

There are a number of non-destructive testing (NDT) methods currently being used to evaluate corrosion problems of concrete structures. In this section visual inspection (VI), half cell, and chain drag will be discussed.

3.1 Visual

VI will be defined in this paper as inspection using the inspector's eyes with no additional equipment except for binoculars and access equipment (i.e. ladder, lift etc.). VI is one of the most widely used inspection techniques and often used to estimate repair quantities for tender. These estimates are often done by "guessing" based on the visible damage. When using VI to detect corrosion, rust stains and potholes are often indicators of advanced corrosion. Staining of the concrete occurs when iron stays in solution and propagates through the concrete causing a red stain, iron oxide, to appear on an outside face. Potholes occur at areas of delamination after the concrete has spalled, often under the action of vehicle traffic. Even with visual signs of corrosion, large areas of damage can go undetected by VI because of the lack of visual indications of corrosion in its initial stages.

VI is a popular technique due to its relatively low cost and the speed at which it can be done. This method is very subjective and the results can be inconsistent (Moore et al., 2001). Numerical rating systems have been developed in an attempt to overcome the subjectivity of VI (Alberta Transportation, 2008). The issue with the numerical rating systems is that they change a rating of good or poor into a numerical value, there is no quantitative definition for good or poor. Even with these rating systems, the results are still inconsistent. A report by the Federal Highway Administration (FHWA) published in 2001 indicates incorrect rating of primary element occurred 56% of the time with a 95% probability. It also concluded that "…only 68% of the population would vary within approximately one rating point from the average" (Moore et al., 2001). One of the biggest benefits of VI is that is can be done at the same time as other inspection techniques and for that reason will remain a staple for DOT's.

3.2 Half cell

The half cell test or reference electrode is a test that takes advantage of the thermodynamic properties of the corrosion process. As corrosion occurs there is an electric current produced between the anode and cathode which results in an electric potential as stated in Chapter 2. When a reference electrode is placed on the concrete surface it can detect this electric potential. The more negative the electric potential the higher the chance of corrosion. This method uses a voltmeter that is connected to the reference electrode and a piece of rebar similar to Figure 2-1.

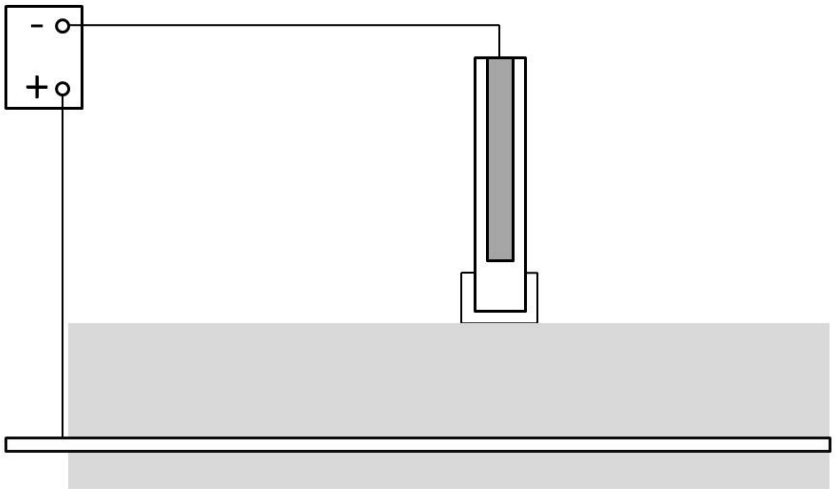

Figure 3-1: Basic half cell setup

Half cell testing does not detect the rate of corrosion or even if corrosion is occurring, it detects an electric potential that can be used to determine the probability of corrosion. For a copper/copper sulfate reference electrode (CSE), passive steel is associated with a potential between +50 and -200 mV. Corrosion due to carbonation is assumed to occur when the potential is between -200 and -500 mV and corrosion due to pitting is assumed when the electric potential is between -400 to -700 mV (Bertolini et al., 2004). ASTM C879-09 is simplified and has three categories; low probability of corrosion, uncertain and high probability of corrosion. When the electrical potential is greater than

-200 mV there is a 90% probability corrosion is not occurring, if between -200 to -350 mV corrosion is uncertain, and a 90% probability of corrosion if less than -350 mV for a CSE. There are a number of factors that can affect the accuracy of this test such as concrete cover and the resistivity of the concrete (Bertolini et al., 2004). This method is also time consuming and requires lane closures. The benefits are it does not require a skilled operator and the equipment is relatively inexpensive.

3.3 Chain Dragging

Chain dragging is a NDT method that conforms to ASTM D4580. It is a commonly used technique for identifying delamination during rehabilitation. The inspection technique uses a chain or hammer that is dragged or struck against the concrete to create a sound; if the concrete is delaminated a "hollow" sound will be produced. Generally chains are used on decks and hammers everywhere else. Figure 3-2 shows chain dragging of a concrete bridge deck during rehabilitation.

Figure 3-2: Chain dragging and delamination marking

This method only detects delaminations, which occur after the formation of corrosion products. Chain dragging is subjective and heavily relies on the operator's skill and experience. Asphalt decks, dirty decks and excessive ambient noise can cause erroneous results because it is difficult to hear and for asphalt decks this method will detect delamination and debonding between the asphalt and concrete (Alberta Transportation,

2007). In addition this method requires lane closures in order to be done safely. It is currently an industry standard for mapping areas to be repaired and is often used as a control for any new inspection techniques.

Chapter 4 Ground Penetrating Radar

GPR is a method of NDT that uses Electromagnetic (EM) pulses to detect subsurface features. A GPR unit consists of an antenna and a control unit. The data acquisition unit converts the computer input parameters into an electric signal. This electric signal is then sent to the antenna where it is emitted as an EM pulse. The pulse reflects when there is a discontinuity in permittivity and the reflected EM pulse travels back to the receiver where it is detected. The control unit then converts the electrical signal into a digital signal. The digital signal is a series of points that makeup the waveform as seen in Figure 4-1; each point provides information on the reflection amplitude and two way travel time (TWTT). The receiver cannot determine the direction from which a returning pulse is coming. The receiver can only measure the time it takes the signal to travel from the transmitter, reflect and come back to the receiver. Given this information and the fact that the antenna is moving, rebar and other small objects will manifest themselves as hyperbolas, Figure 4-1. This occurs because as the antenna gets closer to the rebar the TWTT decreases and the amplitude increases until the antenna is directly over top of the rebar at which point the TWTT starts to increase and the amplitude starts to decrease. A process called migration is used to convert the hyperbolas into a point which is then “picked” and the maximum amplitude and the associated TWTT are recorded. The “picked” amplitude and TWTT are used in the analysis of the structure. The raw data is analysed using software developed by the manufacture called RADAN. RADAN migrates the rebar amplitudes so they can be ‘picked”. Other computer code is required to analysis the amplitude and TWTT to determine whether the concrete is deteriorated. This code was developed as part of the thesis work.

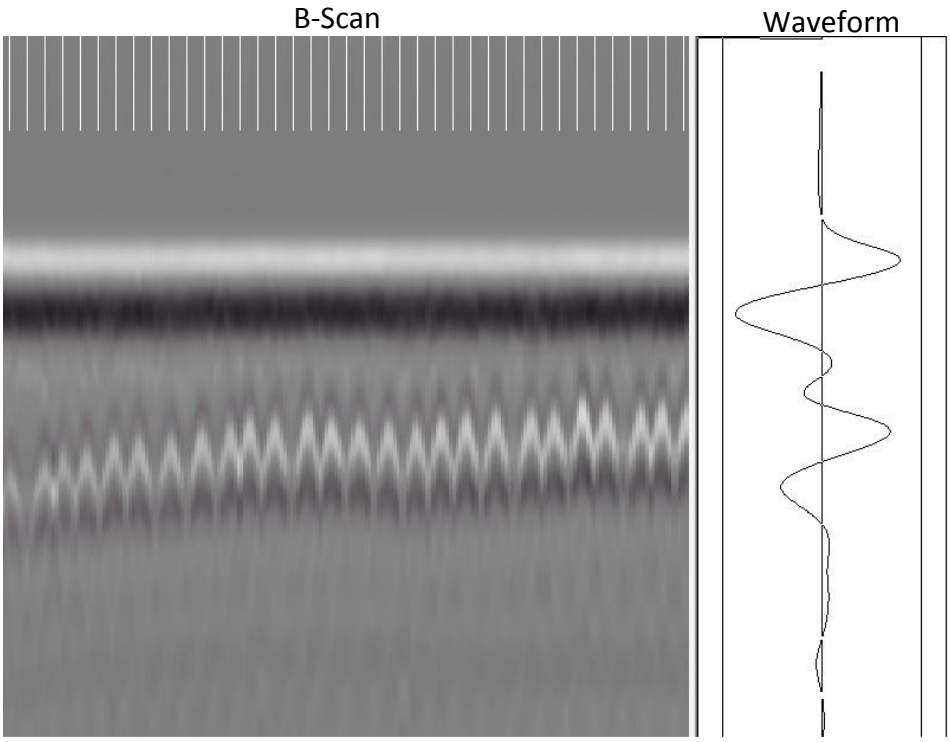

Figure 4-1: B-scan with rebar hyperbolas and waveform

The signal emitted by the GPR's transmitter travels radially outward. Even though the signal travels radially outward it is often modelled through the use of ray paths. Figure 4-2 show the ray paths for a single layer system using a GCA. The top most wave is referred to as the direct wave. It travels directly from the transmitter to the receiver and the only loss that this wave experiences is geometric spreading. The wave just below the direct wave is the surface reflection; this wave has losses due to geometric spreading and the reflection at the air/concrete interface. The superposition of the direct wave and surface reflection is commonly referred to as the direct couple and is the top most reflection in Figure 4-1. The third wave is the rebar reflection. This wave travels from the transmitter through the concrete, reflects off the rebar and is detected by the receiver.

This wave has losses due to geometric spreading, reflection at the air concrete interface, reflection at the rebar and attenuation in the concrete, all of which can be described using electromagnetic wave theory.

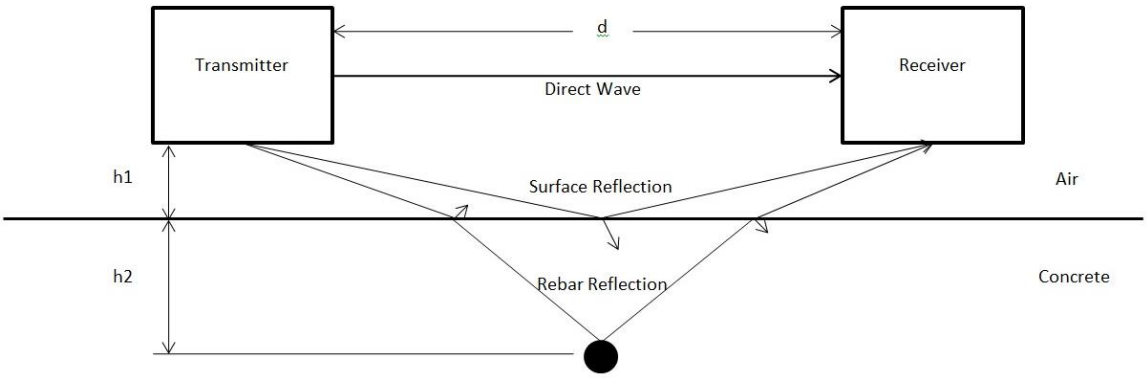

Figure 4-2: Wave travelling

4.1 Electromagnetic Theory

The signal emitted from a GPR antenna is an EM wave, the behaviour of which follows electromagnetic theory. This section provides basic electromagnetic theory and equations used to describe the behaviour of EM waves and pulses in dielectric material (Ulaby et al., 2001). The relevant areas of electromagnetic theory are dielectric permittivity, reflection, velocity of the EM wave and attenuation. These areas in conjunction with the equation for an EM wave result in a model that describes the behavior of an EM wave along individual ray paths.

Dielectric permittivity, ε, is an important electromagnetic material property of the medium in which EM waves propagate. “Permittivity describes the ability of a material to store and release EM energy in the form of electric charge…” (Jol, 2008). The permittivity affects everything from a wave’s velocity to attenuation to the reflection coefficient between different media. It is often described as a complex number as seen

in Equation 4-1, where the real component, ε', represents energy storage and the imaginary component, ε", represents energy loss.

$$\varepsilon = \varepsilon' + j\varepsilon'' \quad \textbf{4-1}$$

Energy storage occurs when an applied electric field passes through a medium causing the atoms to become polarized. This polarization causes a secondary electric field to form, which opposes the applied electric field. Energy loss or attenuation, which is a reduction in the magnitude of the electric field with distance, occurs when any unbound charged particles in a medium, such as chloride, moves due to the applied electric field. As these particles move they collide resulting in energy loss (Jol, 2008). The imaginary component can be related to conductivity, σ, using Equation 4-2, where conductivity is the ability to accommodate the transport of an electric charge (Ulaby et al., 2001).

$$\varepsilon'' = \frac{\sigma}{\omega} \quad \textbf{4-2}$$

ω = angular frequency

There is a magnetic equivalent to permittivity called magnetic permeability, μ. Relative magnetic permeability, μ_r, which is described using Equation 4-3, is assumed to be unity for materials are commonly encountered when using GPR (Ulaby et al., 2001). For this reason the effects of magnetism will not be discussed. It should be noted that this assumption applies to the material that the EM wave travels through, *i.e.* not the reinforcing steel.

$$\mu_r = \mu \cdot \mu_o \quad \textbf{4-3}$$

μ_o = Magnetic permeability of free space

When there is a sudden change in dielectric permittivity a portion of the wave is reflected. The percent reflected and transmitted can be determined using Fresnel's equation for perpendicular waves as shown below (Ulaby et al., 2001).

$$\mathrm{r} = \frac{\sqrt{\varepsilon_{r1}}\cos(\theta_i) - \sqrt{\varepsilon_{r2}}\cos(\theta_t)}{\sqrt{\varepsilon_{r1}}\cos(\theta_t) + \sqrt{\varepsilon_{r2}}\cos(\theta_t)} \quad \textbf{4-4}$$

$$\tau = \frac{2\sqrt{\varepsilon_{r1}}\cos(\theta_i)}{\sqrt{\varepsilon_{r1}}\cos(\theta_i) + \sqrt{\varepsilon_{r2}}\cos(\theta_t)} \quad \textbf{4-5}$$

$$\mathrm{r} = 1 - \tau \quad \textbf{4-6}$$

r = reflection coefficient
τ = transmission coefficient
θ_i = angle of incidence
θ_t = angle of transmission
ε_r = relative permittivity

The angle of transmission can be removed using trigonometric identities and Snell's law, Equation 4-7, to Equation 4-8.

$$\frac{\sin(\theta_i)}{\sin(\theta_t)} = \frac{v_1}{v_2} = \frac{n_2}{n_1} \quad \textbf{4-7}$$

$$\mathrm{r} = \frac{\frac{1}{v_1}\cos(\theta_i) - \frac{1}{v_2}\sqrt{1 - \left(\frac{v_2}{v_1}\sin(\theta_i)\right)^2}}{\frac{1}{v_1}\cos(\theta_i) + \frac{1}{v_2}\sqrt{1 - \left(\frac{v_2}{v_1}\sin(\theta_i)\right)^2}} \quad \textbf{4-8}$$

v = velocity of the EM wave
n = refraction index

For EM waves that have an angle of incidence of zero, Equation 4-9 is used to calculate the reflection coefficient.

$$r = \frac{\sqrt{\varepsilon_{r2}} - \sqrt{\varepsilon_{r3}}}{\sqrt{\varepsilon_{r2}} + \sqrt{\varepsilon_{r3}}} = \frac{\frac{1}{v_2} - \frac{1}{v_3}}{\frac{1}{v_2} + \frac{1}{v_3}} \quad \textbf{4-9}$$

As seen in Equation 4-9 the reflection coefficient can be in terms of relative permittivity of the velocity of an EM wave. This is because the velocity of an EM wave as it travels through a material depends on the permittivity. When calculating the velocity of an EM

wave the real and imaginary components of permittivity must to be separated. Often the imaginary component of permittivity is ignored for low-loss conditions and the velocity equation simplifies from Equation 4-10 to Equation 4-11.

$$v = \frac{1}{\left(\frac{\mu\varepsilon'}{2}\left[\sqrt{1+\left(\frac{\sigma}{\omega\varepsilon'}\right)^2}+1\right]\right)^{1/2}} \quad \textbf{4-10}$$

$$v = \frac{c}{\sqrt{\mu_r\varepsilon_r}} = \frac{1}{\sqrt{\mu\varepsilon}} \quad \textbf{4-11}$$

c = speed of light in a vacuum

The velocity is important because it can be used in conjunction with the TWTT to calculated geometric spreading, where geometric spreading is the reduction in amplitude with distance.

The final source of amplitude reduction is attenuation, α, which is the dissipation of energy as an EM waves travel through a lossy dielectric medium. This means it only occurs in conductive medium.

$$\alpha = \omega\sqrt{\frac{\varepsilon'\mu}{2}\left(\sqrt{1+\left(\frac{\sigma}{\omega\varepsilon'}\right)^2}-1\right)} \quad \textbf{4-12}$$

The losses due to reflection, geometric spreading and attenuation are incorporated into the electromagnetic wave equation. Maxwell's equations, Equations 4-13 to 4-16, describe the relationship between electric and magnetic fields which are used to derive the differential equations that describe electromagnetic waves, Equations 4-17 and 4-18.

$$\nabla \cdot E = \frac{\rho}{\varepsilon_o} \quad \textbf{4-13}$$

$$\nabla \cdot B = 0 \quad \textbf{4-14}$$

$$\nabla \times E = -\frac{\partial B}{\partial t} \quad \textbf{4-15}$$

$$\nabla \times B = \mu_o J + \mu_o \varepsilon_o \frac{\partial E}{\partial t} \quad \textbf{4-16}$$

$$\left(\nabla^2 - \mu\varepsilon \frac{\partial^2}{\partial t^2}\right) E = 0 \quad \textbf{4-17}$$

$$\left(\nabla^2 - \mu\varepsilon \frac{\partial^2}{\partial t^2}\right) B = 0 \quad \textbf{4-18}$$

∇ = Gradiant
E = Electric Field
B = Magnetic Field
ρ = Charge density
t = time
J = Current Density

The solutions to the differential equations are:

$$E(r,t) = E_o e^{j\beta z} e^{-j\omega t} \quad \textbf{4-19}$$

$$B(r,t) = B_o e^{j\beta z} e^{-j\omega t} \quad \textbf{4-20}$$

β = Phase constant (rad/m)
E_o = Initial Electric Field
B_o = Initial Magnetic Field

Equations 4-19 and 4-20 describe the amplitude of the electric and magnetic field, respectively, as a function of time, t, angular frequency, ω, and distance, z. The general EM wave equation for a single layer system is given by Equation 4-21, which includes the effect of attenuation, reflection and geometric spreading

$$E(z,t) = E_o e^{j\beta z} e^{-j\omega t} e^{-\alpha z}\, r_{12} r_{21}\, G(x) \quad \textbf{4-21}$$

G(x) = geometric spreading

When modeling GPR signals only maxima, and corresponding minima, are going to be considered. This will simplify the EM wave model by removing the location and time components of the general EM wave equation, resulting in Equation 4-22. This model is applicable for a signal layer system like concrete and would follow the rebar reflection

ray path as seen in Figure 4-2. More comprehensive models will be presented for multilayer systems in Chapter 9.

$$E(z,t) = E_o e^{-\alpha z}\, r_{12} r_{21}\, G(x) \qquad \textbf{4-22}$$

4.2 Literature Review

This section explores the development of using GPR as an assessment tool for concrete bridge decks with a focus on asphalt overlaid decks. It starts with the history of using GPR to evaluate deterioration of concrete bridge decks, first looking at variations in amplitude and travel time of the returning signal without any adjustments (Holt, 1982; Clemeña, 1983). Continues by looking at research that focused on analysing variations in the asphalt concrete interface and rebar amplitude (Maser, 1991; Alongi at. el. 1992) and finishes with a method that accounts for geometric spreading (Barnes at. el., 2008). In addition to looking at evaluation methods, methods for calculating permittivity, geometric spreading, reflection, attenuation, and the use of GCA's on bridge desks are explored.

4.2.1 Methods/Evaluation

There are a number of ways to identify deterioration of concrete using GPR. These methods include variation in TWTT, variation in the reflection amplitude, and attenuation.

In 1982 Holt published a paper on different inspection techniques for detecting deterioration on bridge decks; one of which was GPR. He noticed that deteriorated concrete could be identified by an increase in the asphalt concrete interface reflection amplitude. Unfortunately this method only detected 51% of the delaminations and was only able to accurately predict the condition of the concrete 26% of the time. Around the same time Clemeña (1983) tried to identify deteriorated concrete by locating time

delays of the asphalt concrete interface reflection amplitude and was met with limited success.

Maser (1991) used the asphalt concrete interface reflection to calculate the permittivity of concrete in order to predict delamination on asphalt overlaid bridge decks using an air coupled antenna. The permittivity of concrete was calculated using Equation 4-23 which uses the permittivity of asphalt and the ratio of the surface reflection and the interface reflection, R_2. Maser was able to successfully detect the quantity of delaminations with an average error of 3% for 26 structures.

$$\varepsilon_c = \varepsilon_a \left[\frac{(F - R_2)}{(F + R_2)}\right]^2 \quad \textbf{4-23}$$

$$F = \frac{4\varepsilon_a^{0.5}}{1 - \varepsilon_a} \quad \textbf{4-24}$$

Variation in TWTT, variation in the asphalt concrete interface and the attenuation of the signal were investigated as means of identifying concrete deterioration by Alongi et. al. (1992). This research was conducted on asphalt overlaid bridge decks without a waterproof membrane using an air coupled antenna. Success was achieved in identifying deterioration using the asphalt concrete interface reflection similar to Maser (1991). However, attenuation as a means of deterioration detect was favoured because it was more accurate and attenuation only occurs if the conditions that allow corrosion are present, chloride and moisture.

There is some evidence that the type of deterioration on asphalt overlaid bridge decks can be determined when using an air coupled antenna (Chung et. al. 1992). Chung included the effects of reflection and geometric spreading on the amplitude of the EM wave. Noise was removed by holding the antenna in the air and subtracting that from the recorded waveform further improving the results. The surface reflection was used to

determine the permittivity of asphalt which was then used to account for geometric spreading. It was noticed that the permittivity changes over the surface of the deck and for this reason permittivity was calculated for each scan. The concrete cover was determined using a non-conductive model where the permittivity of concrete was assumed. This paper focused on using the GPR to detect existing damage such as scaling, debonding and delamination. Scaling and debonding occur at the concrete asphalt interface which does not require the EM wave to be modeled in concrete. With respect to delamination this paper looked at how the cracks affected the signal but ignored the effects of attenuation.

In 2004 Barnes was successful in using an air coupled antenna to detect deterioration using a visual inspection of the collected GPR waveforms. Deterioration was identified by high interface reflection amplitudes, similar to Maser's method, or low rebar reflection, attenuation. Barnes found that GPR, when using an air coupled antenna, produced the most accurate area estimates on bridges deck where the damage to the deck was between 10 to 50% of the total deck area, as determined by chain dragging.

4.2.2 Permittivity

Multilayer systems require the consideration of reflection loss at the interfaces and surface as well as the attenuation within the asphalt layer in addition to geometric spreading. The reflection losses and geometric spreading can be accounted for provided the permittivity of the top layer (asphalt for multilayer deck systems) is known. There are a number of methods for determining the permittivity of concrete and asphalt which includes coring and analysis of the surface reflection. Determining the permittivity from cores is done using Equation 4-11, where the velocity is determined using the TWTT obtained from the GPR and the height of the core. The surface reflection uses Fresnel's equation, Equation 4-4, where the relative permittivity of air, ε_{r1}, is assumed to be one. Using cores to calculate the permittivity has proven to be the most successful method for accurately determining the depth of concrete/asphalt with the surface reflection as a close second (Loizos & Plati, 2006). One of the reason cores are the most accurate way

of determining permittivity is that cores are used as the control when evaluating the accuracy of the estimated permittivity. As well the TWTT will produce the “average” permittivity of the medium because the EM wave is affected by the entire depth of the medium not just the surface.

Many papers have been written on determining the depth and thus permittivity of roads using the surface reflection from an air coupled antenna (Al-Qadi & Lahouar, 2005;Lahouar & Al-Qadi, 2008;Loizos & Plati, 2006;Maser, 1994). The methods described in these papers have had good success in predicting the depth of the asphalt and the base layer.

One paper reported being able to predicted the thickness of asphalt and base layers within ± 7.5% and ± 12 %, respectively (Maser, 1996). Maser’s model again uses Fresnel’s equation in conjunction with the surface and interface reflection to calculate permittivity. The asphalt is treated as a non-conductive medium and the base is treated as a conductive medium (Maser, 1994). Maser has also predicted the depth of concrete using the surface reflection; Figure 4-3 shows that the depth of asphalt can accurately be determined using the surface reflection whereas concrete has less accurate results (Maser, 1994).

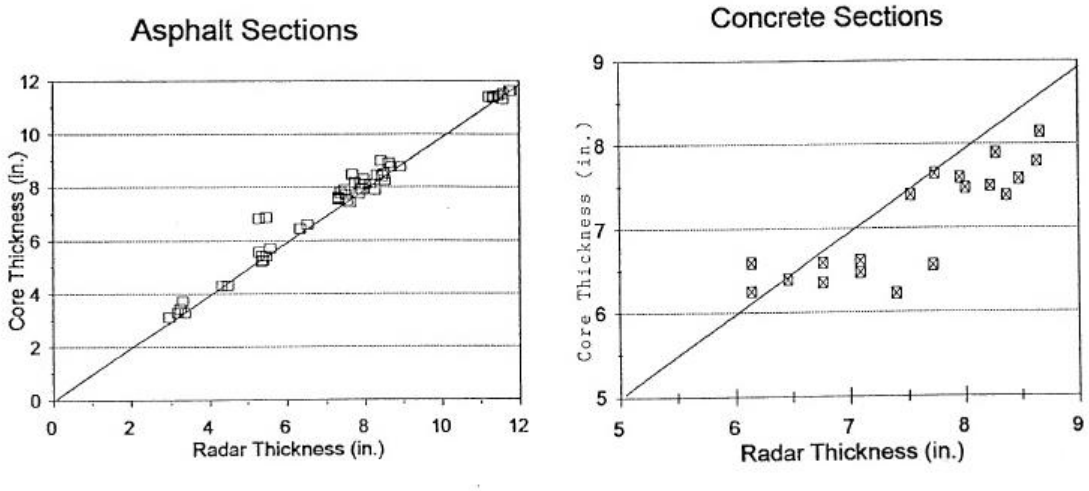

Figure 4-3: Radar thickness vs. core thickness for concrete and asphalt (Maser, 1994)

Chung (1992) also had success in determining the permittivity of asphalt using the surface reflection of an air coupled antenna. The permittivity of asphalt determined using the surface reflection was able to predict the thickness of asphalt within 5% to 8%, where the actual thickness was determined using cores. In 1994 Chung et. al. again tried to predict the permittivity using the surface reflection and compared that to the permittivity determined using cores and the time delay. The resulting permittivities were within 7.8% using a non-conductive model for asphalt.

The surface reflection is a desirable means of determining permittivity because it can be done over the entire survey area and does not require destructive tests such as coring.

4.2.3 Geometric Spreading

Geometric spreading is the loss in signal amplitude based on the distance from the source. The best analogy is throwing a stone into a pond, as the wave travels out from the point of "impact", or the source, the height of the wave reduce. It should be noted that the amplitude changes with distance but not result in a change to the total energy in the wave. EM wave follow the same principle.

In 1992 Chung accounted for geometric spreading through a calibration factor (Chung et al., 1992). The calibration factor was determined by placing the antenna at different heights above a metal plate and recording the voltage. A chart was created that had voltage on one axis and distance on the other. Chung states that the spatial losses of asphalt can be approximated by multiplying the square root of the asphalt permittivity. It is unclear what the square root of the permittivity is being multiplied by. Examples are given in the paper and it appears Chung is multiplying the square root of the permittivity by the asphalt thickness. In the examples the permittivity is close to six resulting in a square root value near two and one half. This suggests that the antenna is a point source where the geometric spreading will be 1 over the distance travelled or twice the thickness. Chung was able to predict the thickness of asphalt within ± 8 % using the calibration factor.

Barnes et al. (2008) accounted for geometric spreading of a GCA signal on unpaved reinforced concrete decks by normalizing the rebar amplitude data, in dB, to the 90th percentile of the rebar amplitude data, in dB, when plotted against TWTT. This method was able to predict the repair area within 3% for bare decks. The benefit of this method is that the depth of the rebar does not need to be known only the TWTT and amplitude of the rebar reflection which are provided by the GPR unit directly. Geometric spreading is the only source of loss that needs to be removed for bare concrete decks because the losses due to the reflection at the surface and at the rebar are reasonably assumed to be constant leaving attenuation as the only cause of variation in rebar amplitudes. Even with all the research into the effects of geometric spreading, the ASTM standard D6087 – 08, which outlines the use of GPR for evaluating bridge decks, does not consider the effects of variation in rebar depth. It focuses on differences in amplitudes in effect assuming any variation in amplitude is due to attenuation.

4.2.4 Reflection

There is some disagreement when it comes to the significance of conductivity on the reflection coefficient. Equation 4-4 does not consider the effects of conductivity. In order to do that a complex reflection coefficient equation must be used. Maser (1991) suggested that the reflection coefficient is “significantly” influenced by the conductivity. It should be noted the Maser only considered the complex reflection coefficient at the asphalt concrete interface and not the surface reflection.

Alongi at. el. (1992) states that the reflection coefficient is not “significantly” affected by the conductivity that would be expected on bridge decks. Their conclusion was the result of laboratory tests conducted using sand as a substitute for concrete, water and salt.

In 1994, Chung et. al. conducted tests to develop a model that recreated GPR waveforms. During analysis the surface wave was removed in an attempt to improve the accuracy of the model. The surface wave was removed by subtracting a theoretical waveform from the actual waveform. When this subtraction was done it was noticed

that there was “noise” in the shape of the source wave. Upon further investigation it was determined that this “noise” was a result of conductivity and a complex reflection coefficient was able to remove the “noise”. The use of a complex reflection coefficient was able to predict the depth of a sample with rebar within 3 %.

It should be mentioned that Chung and Maser only recommended a complex reflection coefficient when the EM wave reflected off concrete. For asphalt the reflection coefficients that were used are consistent with Equation 4-4 except that the angle of incidence is assumed to be zero because air coupled antennas were used.

4.2.5 Attenuation

Attenuation is the loss of energy from the EM wave due to the motion of free ion within the medium. Attenuation was one of the first indicators considered for detection of deterioration using GPR. Early condition assessment methods used a qualitative attenuation approach that would assume corrosion was occurring if the rebar reflection amplitude was “weak”; more advanced methods used a threshold value. These approaches gave widely varying results because it assumed the only source of loss was attenuation. As stated above Barnes (2008) improved the accuracy of the attenuation method by removing variation in signal amplitude due to rebar depth.

Alongi et al. (1992) used sand to try and determine the effects of moisture and chloride on GPR signals. They found that moisture affected the reflection coefficient and signal velocity whereas chloride content had a significant effect on attenuation. They also noticed that moisture needed to be present for chloride to cause attenuation. Out of the method for indicating deterioration that Alongi tested, which included attenuation, interface reflection and TWTT, attenuation was the most accurate with the interface reflection a “close” second (Alongi et al., 1992).

4.2.6 Ground Coupled Antenna

Two papers were found that attempted to use a GCA on asphalt overlaid deck. Billington (2003), in his report GPR surveys to help determine condition of a concrete bridge deck, used a 1.5 GHz GCA to evaluate the deterioration of an asphalt overlaid bridge deck.

Without correcting for depth Billington grossly overestimated the deterioration at 97% of the deck area using a constant threshold value of -14 dB. It was noticed that the signal strength varies with TWTT or depth. When the variation in rebar depth was corrected and using a new threshold value used, the estimated deteriorated area was 45% of the deck.

Romero (2000) also used a 1.5 GHz antenna to evaluate an asphalt overlaid bridge deck. The goals of this project included identification of deterioration and determining the level of deterioration and boundaries. The first analysis used GSSI's recommended -10 dB threshold values resulting in a large total repair area. The threshold value was adjusted to -15 dB and anything between -14 to -15 dB that also showed signs of deterioration through visual inspection was identified as deteriorated. This method did not correct of variations in asphalt thickness, rebar depth or reflection at the concrete asphalt interface.

4.3 Research Model Outline

Evaluation of concrete deterioration on bridge decks using GPR up to this point has identified areas as damaged or not. The next step in the research is to develop a method for determining the level of damage in concrete using a variable with physical meaning. The variable that was chosen is conductivity. Conductivity is related to attenuation and chloride content (Alongi et al., 1992). The relationship between conductivity and chloride contend was further confirmed by Sketchley (Sketchley et al., 2014). Sketchley was also able to correlate threshold levels of conductivity with damage. In order to calculate conductivity the losses due to attenuation need to be isolated which can be done by calculating and removing the geometric spreading and reflection losses.

The first step is to determine the appropriate geometrics spreading model for the antenna used. Once the geometric spreading model is determine a method for determining the permittivity of the top layer using a GCA will be investigated. The final step is to develop and verify an EM wave model for a multilayer system.

The EM wave models developed in this thesis are based on Equation 4-22 which accounts for geometric spreading, reflection and attenuation. The reflection coefficient will be non-complex for reasons of simplicity. Concrete will be treated as a conductive medium, with the exception of one method, and the conductivity of concrete will be calculated. A GCA will be used because it has a smaller “footprint” which will result in a high resolution image allowing individual rebar to be analysed. The direct couple will be used in all models proposed for multilayer systems. The main difference between the methods proposed in this thesis was whether or not the asphalt was considered conductive and the techniques used to solve the system of equations.

Chapter 5 Equipment and Testing

The GPR unit that was used was a GSSI SIR-20 with a Model 5100 GCA which has a central frequency of 1.5 GHz as seen in Figure 5-1. A Model 5100 GCA is a dipole antenna with a fixed transmitter/receiver (T-R) spacing of 58 mm, as reported by the manufacturer. It should be noted that the 58 mm T-R spacing is not a measured value, it is determined through tests conducted by the manufacturer. Before any testing the equipment was allowed to "warm up" for the manufacturer's recommended 30 minutes. This is done to allow the output signal stabilize. If this step is ignored the amplitude of the returning signal may vary due to a variation in the output signal.

Figure 5-1: Radar equipment used for testing

When conducting laboratory tests, the direct wave data was collected before and after each sample to monitor signal variation. In addition to collecting direct wave data, during testing of laboratory samples the antenna was moved back and forward to get an "average" reading. When conducting field tests on bridge decks, the survey lines were positioned 0.5 m apart across the width of the deck with the first one being 0.25 m away

from the curb face. These survey lines were positioned along the length of the deck in order to orthogonally cross the uppermost layer of transverse reinforcing steel. The sample and scan rate differed depending on the test being performed. The standard system sample rate was 512 samples/scan with a scan rate of 200 scans/sec.

The research program consisted of a number of different tests, the first being a test to determine the appropriate geometric spreading model. This test used polystyrene sheets to provide a known distance between the antenna and the reflective metal surface. The number of 51 mm polystyrene sheets varied from zero to 8 resulting in the antenna being at a maximum height of 406 mm above the metal plate.

The second test that was conducted attempted to use the direct couple from a GCA to determine the permittivity of asphalt and concrete. Six test samples were made of asphalt and eight test samples were made of concrete. The asphalt samples came from a laboratory at Dalhousie University and the concrete samples consisted of HPC, Class C and Tremie Pile concrete that were made in accordance with Alberta Transportation specifications. The thickness of each sample was measure in order to calculate the actual permittivity of each sample.

The third test was the field test for the determining the permittivity using the surface reflection of a GCA. Previously collected data from four bridges in Nova Scotia was used, all of which had bare concrete decks. These bridges were located near Milford, West River, Shubenacadie, and Sambro. In this set of tests the conductivity calculated using the surface reflection method was compared to the conductivity calculated using a method developed by Sketchley et. al. (2014).

The fourth test used previously collected data from three asphalt overlaid bridge decks located in Nova Scotia which were located near Musquodoboit, Shediac, and Bedford. The conductivity of the concrete was calculated of each structure and compared to chain dragging and half cell results, where available. When there was no half cell or chain dragging data the conductivity and permittivity were reviewed to see if there magnitudes were within an acceptable range.

Chapter 6 Experimental Modeling of Geometric Spreading

Geometric spreading describes how an EM wave weakens as it diverges from its source. Equations for geometric spreading have been developed for both point sources and line sources. No information was available as to whether the antenna used in the tests should be modelled as a point or line source.

6.1 Testing

The test consisted of stacking 51 mm polystyrene sheets on top of one another with a sheet of metal underneath. The first set of data was collected with the antenna on one sheet of foam and from there the height was increased incrementally by 51 mm to a maximum nominal height of 406 mm. The system was set at 200 scans/sec and 512 samples/scan with no gain.

6.2 Results and Analysis

The analysis consisted of plotting the amplitude ratio vs. the distance ratio calculated using Equation 6-1 below, where A_r is the reference amplitude at some distance x_r from the source and A_i is the amplitude at some distance x_i from the source. Equation 6-1 is the relationship of a point source.

$$\frac{A_r}{A_i} = \frac{x_i}{x_r} \qquad \textbf{6-1}$$

Figure 6-1 shows the relationship between the amplitude and distance ratio, where the reference wave is fully contained within the foam. The relationship is approximately linear with a slope approximately equal to one. This relationship is expected for a point source.

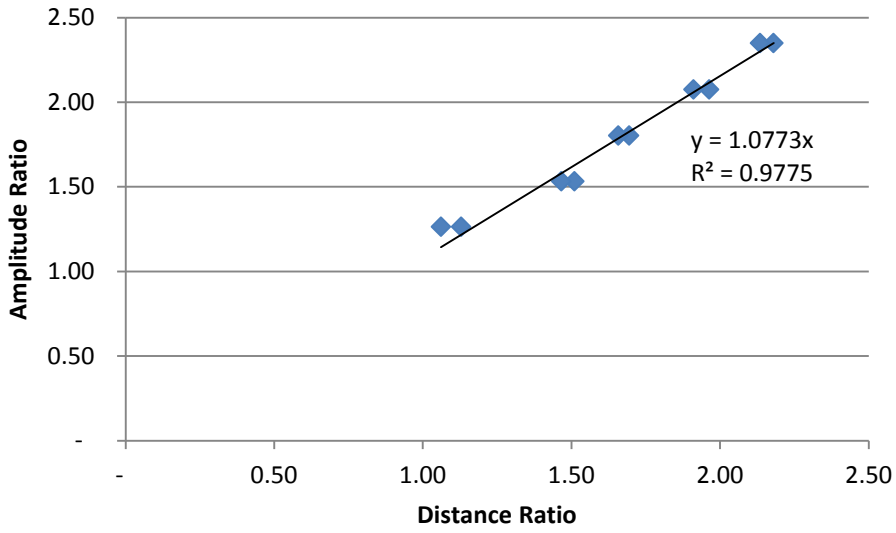

Figure 6-1: Geometric spreading from a point source

In Figure 6-2 the direct wave was taken as the reference wave with a transmitter receiver (T-R) spacing of 92.5 mm. The slope is linear but not equal to one. The approximately linear slope indicates that the geometric spreading can be modelled using a modified version of the generally accepted point source equation by including a correction factor, ϕ, which is equal to the slope of the line in Figure 6-2.

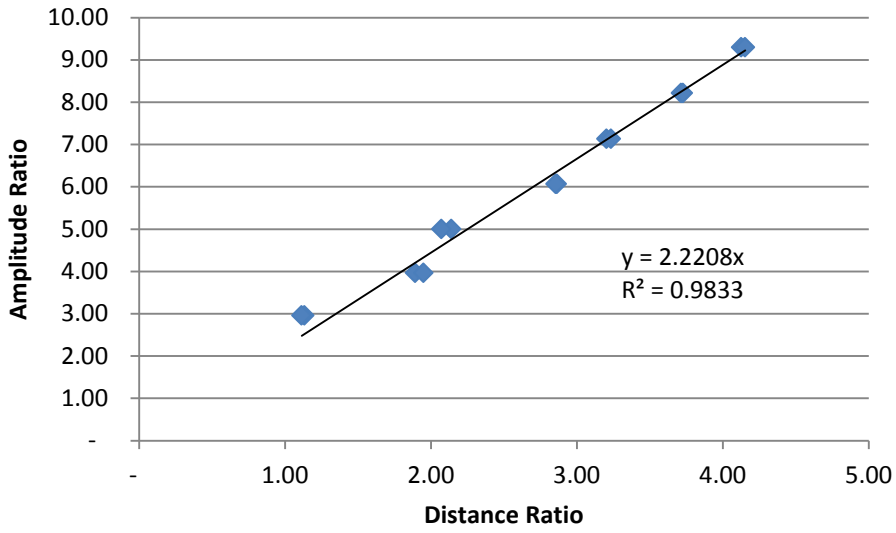

Figure 6-2: Geometric spreading from a point source, with the direct wave as the reference wave

6.3 Discussion

In general, the geometric spreading can be modelled as coming from a point source. When the reference wave is the direct wave a correction factor is needed. It is possible that a correction factor is required because the T-R spacing may be greater than 58 mm, which is determined by GSSI (GSSI, 2007), far field equations are used in the near field, or because of internal reflections. If the spacing of the T-R is not 58 mm then the geometric spreading model developed above will not produce the correct results because the reference distance is incorrect. The effects of the T-R spacing on the correction factor can be seen in Figure 6-3, which show the correction factor decreasing with an increase in T-R spacing. Figure 6-3 was produced by numerically adjusting the T-R spacing and recording the corresponding slope, the correction factor, as seen in Figure 6-2. The T-R spacing does not fully explain the need for the correction factor because at the physical maximum spacing of 170 mm there is still a correction of 1.5.

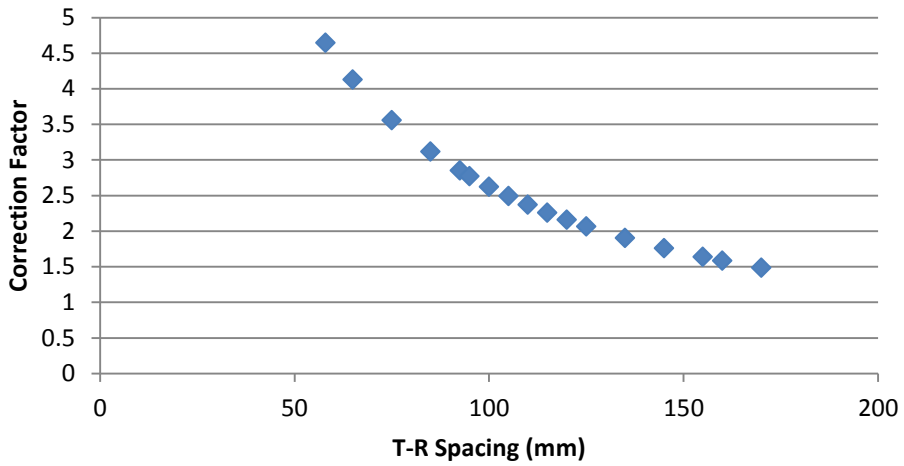

Figure 6-3: Change in correction factor with respect to T-R spacing

Another possibility is that the correction factor is accounting for variations between the behaviour of an EM wave in the near and far fields; the equations used for geometric spreading assumes far field behaviour. In the far field the EM wave can be modelled as a plane wave but this is not accurate in the near field. There are two types of near field, the reactive and radiative. If the T-R spacing is 58 mm, the receiver is outside the reactive near field but still within the radiative near field as defined for an electromagnetically short antenna (OSHA, 1990). This means that there is no interaction between the transmitter and electric field, as would be in the reactive field, but the EM wave cannot be modelled as a plane wave, as in the far field. Internal reflection within the antenna casing could result in the need for a correction factor. Possible sources of internal reflection within the antenna include debris within the antenna house, the antenna housing itself, components of the antenna wiring and survey wheel among others. Internal reflections cannot be ruled out at this point, but like the near field this does not matter as long as the effect remains constant and can be accounted for with the correction factor. The correction factor allows the direct wave to be used as the reference wave, and is both easily obtained and is relatively constant.

Chapter 7 Surface Couple

Permittivity is an electromagnetic material property that can be used to determine depth, conductivity and water content of concrete and asphalt. Currently air coupled antennas use the surface reflection to determine permittivity. This is not possible for GCA because there is interference between the surface reflection and direct wave. This section proposes a method for determining the permittivity of the top layer by isolating the surface reflection from a GCA.

7.1 Theory

The method for calculating permittivity is dictated by the type of antenna used. Air coupled antennas are able to calculate the permittivity of the top layer using the surface reflection, Fresnel's equation and a metal plate. The metal plate is placed on the ground and a reading is taken at a specific height. During testing the amplitude of the surface reflection is obtained from the uppermost layer and the permittivity of the top layer is calculated using Fresnel's equation, assuming the permittivity of air is 1. The permittivity of the top layer cannot be calculated using a GCA because of the interference between the direct wave and the surface reflection. Research has shown a relationship between the amplitude of the direct coupling wave and the amount of chloride and moisture in concrete (Sbartaï et al, 2006).

In order to use the surface reflection of a GCA it needs to be isolated from the direct couple. The direct couple may be assumed to be the superposition of the wave that travels directly from the transmitter to the receiver (direct wave), internal antenna reflections, and a wave that interacts with the interface between air and pavement layer (surface reflection). It should be noted that there is a "thin" layer of plastic separating the antenna from the pavement, and according to the manufacturer the plastic has little effect on the signal. The direct wave and internal reflections are measured from the data recorder while holding the antenna in the air. If the direct wave and internal reflection are assumed to be constant and the direct couple follows the principle of superposition, the surface reflection may be isolated by subtracting the direct wave and

internal reflections from the direct couple. Once the surface reflection has been isolated the question is whether the wave reflects at the air/asphalt interface or whether the wave travels along the interface.

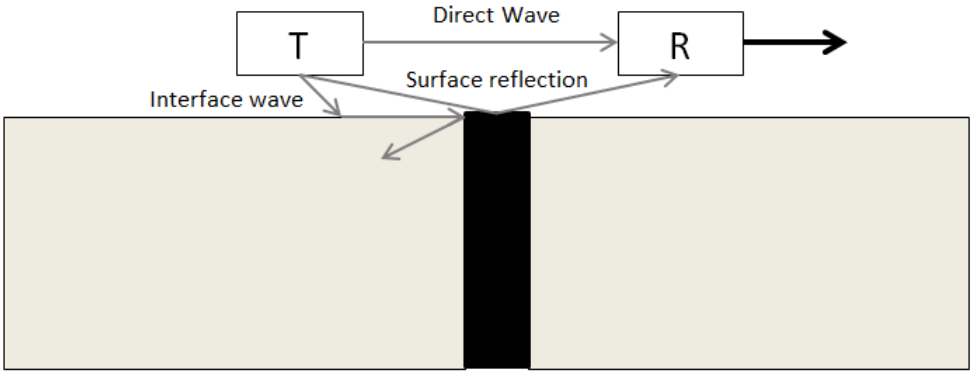

Figure 7-1: Test to determine whether there is a surface reflection or the wave travels along the air concrete interface

In this paper it is assumed that the surface reflects the wave for two reasons. The first is that the amplitude of the direct couple decreases when the antenna is placed on a material with a permittivity higher than air; this can be explained because the reflected wave undergoes a 180 degree phase shift. Secondly when a metal plate is placed between two asphalt samples and the antenna is moved from one sample to the other over the plate there is no significant change in the amplitude of the direct couple, as seen in Figure 7-1. If the surface reflection traveled along the air/asphalt interface then the metal plate should have prevented the wave from reaching the receiver resulting in a change of signal as the antenna moved from one sample to the other. Since the wave is reflected at the surface Fresnel's equation can be used to determine the permittivity of the top layer.

7.2 Sample Preparation and Testing

Asphalt and concrete samples were used in a laboratory test using asphalt samples found in a laboratory at Dalhousie University, that were used in a previous PHD thesis (Barnes, 2008). The concrete samples were collected from a bridge construction site in Calgary, Alberta. The concrete samples are approximately 300 mm by 460 mm by 85 mm. Three classes of concrete were used that conform to Alberta Transportation Specifications; HPC, Class C, and a Tremie Pile mix. The samples were collected on site using the left over concrete from slump and air entrainment tests. The samples were finished using a steel hand trowel and were left on site for a minimum of 2-3 days to allow the concrete to cure before being moved to be tested in a temporary laboratory.

Each sample was tested for approximately 15-30 seconds with a maximum of 5 samples per file. As a control, the same three samples were tested at the beginning of each file. The radar settings were 512 & 2048 samples per scan, 39 scans/second and a range of 8 ns. The samples per scan were chosen as 512 and 2048 because 512 is the default used in field applications and 2048 was used to see if the number of samples per scan affected the results. The reason 39 scans/second was the maximum scan rate the system would allow for a 2048 sample rate.

7.3 Analysis and Results

The analysis consists of first isolating the surface reflection, then using Fresnel's equation to determine the permittivity. Isolation of the surface reflection was done by subtracting the direct wave, A_{air}, from the direct couple. Initially this was done by collecting direct wave data at the beginning and end of each file. The average amplitude and time of the direct waves was calculated and used to identify a single direct wave in the file with the same average amplitude and time. This selected wave was then subtracted using the background removal function in the RADAN software. This method was labour intensive and required each file to be analysed individually. In order to improve the efficiency and eliminate the need to collect direct wave data, the surface

reflection was plotted against the direct couple as seen in Figure 7-2. The relationship between the direct couple and surface reflection is linear with a slope very close to one.

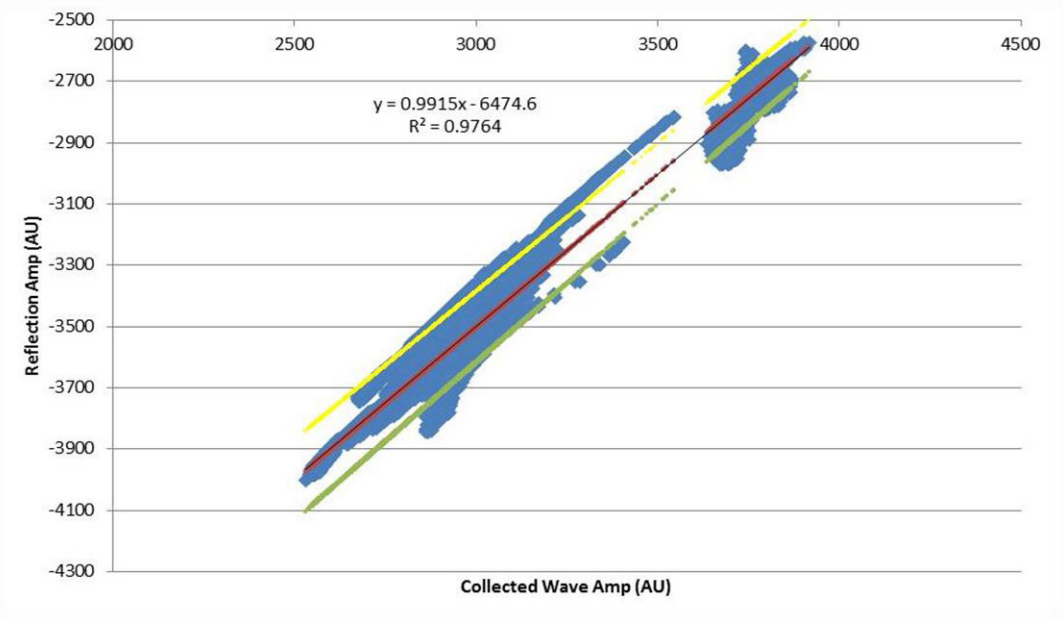

Figure 7-2: Surface reflection amplitude vs. direct couple amplitude

When the slope is assumed to be 1.0 the amplitude of the surface reflection can be predicted within 3.25%, 95% of the time. This was deemed accurate enough to eliminate the need to collect direct wave data. The two lines in Figure 7-2 near the extremities of the data represent an offset of ±3.25% from the predicted reflection amplitudes, or the centerline. The equation in Figure 7-2 should be constant provided the GPR settings are constant. This is because the equation is subtracting the direct wave from the direct couple and the direct wave is constant.

Once the surface reflection was isolated, Fresnel's equation was used to calculate the velocity of the EM wave in the top layer. Since the antenna is close to the ground it was assumed that the incident angle was greater than 0 degrees which, requires the use of Equation 7-1 (Ulaby et al., 2001).

$$r = \frac{\frac{1}{v_1}\cos(\theta_i) - \frac{1}{v_2}\sqrt{1 - \left(\frac{v_2}{v_1}\sin(\theta_i)\right)^2}}{\frac{1}{v_1}\cos(\theta_i) + \frac{1}{v_2}\sqrt{1 - \left(\frac{v_2}{v_1}\sin(\theta_i)\right)^2}} = \frac{\max(A_{wave\,2'})}{\max(A_{wave\,2})} \quad \textbf{7-1}$$

$$A_{wave\,2} = \emptyset\, A_{air} \sin(\theta_i) \quad \textbf{7-2}$$

$$v = \frac{2 * \sqrt{\left(\frac{58}{2}\right)^2 + (depth)^2}}{TWTT} \quad \textbf{7-3}$$

$A_{wave\,2}$ is the amplitude just prior to reflection and is calculated using Equation 7-2. $A_{wave\,2'}$ is the amplitude just after reflection which is the surface reflection that is recorded. The angle of incidence was determined through an iterative process that minimized the error between predicted velocity and the actual velocity of the EM wave in the sample. The actual velocity was calculated using Equation 7-3 utilizing the known depth of the layer and Equation 7-1 was rearranged to calculate the predicted velocity using the average angle of incidence. The predicted and actual velocities were compared by calculating the 95th percentile of the absolute error. The absolute error was minimized by adjusting the T-R spacing. The error was minimized to approximately 4% error 95% of the time for a T-R spacing of 92.5 mm, possible reasons for the discrepancy between the 92.5 mm T-R spacing and GSSI's 58 mm T-R will be discussed in section 7.4. Figure 7-3 compares the actual velocity and the predicted velocity. With a slope of approximately one and an R^2 of 0.98 it can be concluded that the model is able to accurately predict the velocity of an EM wave. The two groups of data, upper (green) asphalt and lower (red) concrete, have similar levels of accuracy indicating the model is independent of the material tested.

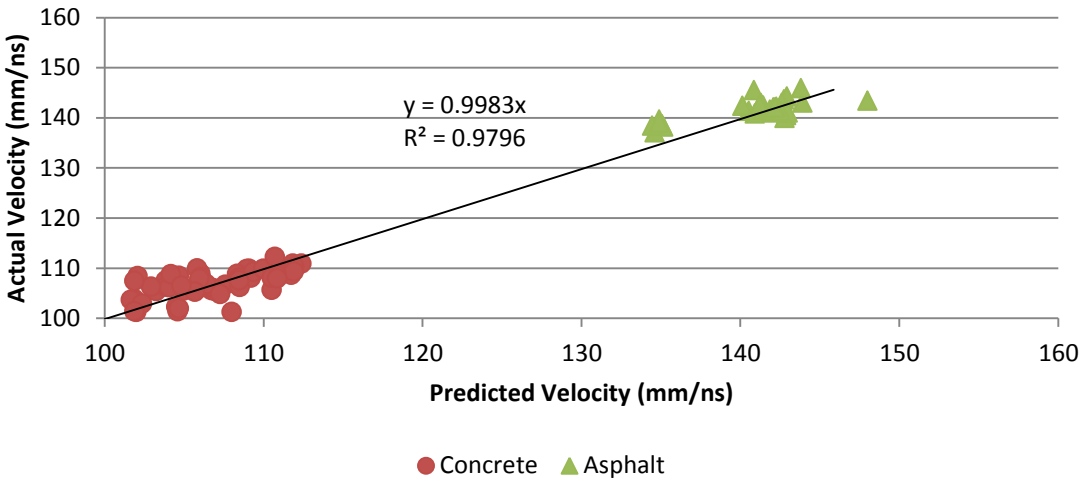

Figure 7-3: Predicted and actual velocity of EM wave in laboratory samples

7.4 Discussion

The question that arises from the above method is: how well does surface permittivity relate to bulk permittivity in the field? Such things as debris, overlays, cracks, and the distribution of moisture within a layer may all cause a variation between surface permittivity and the bulk permittivity. However in this research it was assumed that permittivity was constant for simplicity.

It should be noted this method is an approximation and the equations may produce result that do not have physical meaning. One such example is the antenna's height above the ground which is calculated to be 110 mm; based on physical measurements the antenna height is no more than 70 mm. The equations are representative of the far field but are being used in the radiative near field. The experimental data indicates that this is an acceptable assumption. Any error caused by misusing far field equation seems to be corrected by the correction factor found in the geometric spreading tests. If the error is constant for each EM pulse then a simple correction is reasonable.

The variation in the "standard" T-R spacing of 58 mm, as determine by the manufacturer and the calculated T-R spacing, 92.5 mm, determined from error minimization is unclear. The only area that would be affected by the T-R spacing and not the correction

factor is the angle of incidence. The angle of incidence, in this case, is the angle at which the EM wave interacts with the uppermost surface interface. After a discussion with an employee of GSSI Roger Roberts (personal communication, April 2014), which manufactured the equipment, it appears that the direct couple is a combination of the direct wave, surface reflection and surface waves. These surface waves were ignored in the analysis and may account for the discrepancy between the 58 mm started by GSSI and the calculated 92.5 mm. The 92.5 mm T-R spacing could account for the surface wave because the 92.5 mm spacing would produce a larger angle of incident and thus a larger reflection coefficient. The larger reflection coefficient would allow for the amplitude of the surface reflection and surface waves to combine yet still accurately predict permittivity assuming solely a surface reflection.

Although the above method was done without collecting the direct wave for each file, it is the author's recommendation that the direct wave data still be collected in order to calibrate for gain and as a check to ensure the equipment is operating properly. The gain check is done by calculating the gain using the average of the direct wave data collected during testing, A_{test}, and the average amplitude of the direct wave with no gain applied, A_{ref}, using Equation 7-4. The direct wave data will also ensure the equipment is operating correctly because the direct wave should be constant and if there is a significant variation between the start and end of the test the equipment may have malfunctioned. This could mean that variation in the amplitude of the direct couple, interface reflection or rebar reflection is due to variation in signal output and not material properties.

$$Gain(dB) = 20\log\left(\frac{A_{test}}{A_{ref}}\right) \qquad \textbf{7-4}$$

Chapter 8 Single Layer

The semi-infinite half space of air in which the antenna exist is common to all models. Therefore a single layer system will be defined as a model with only a layer of concrete beneath the antenna space. This section outlines and tests a procedure that uses the surface reflection from a GCA to determine the conductivity from GCA data collected over the surface of a bridge deck. This method will be compared to another method that does not use the surface reflection to calculate conductivity, which will be referred to as the control method (Sketchley et al., 2014).

All the structures analysed in this section are bare concrete decks. Complete details of the structures and collection of raw data can be found in Redmond (2007).

8.1 Analysis and Results

In a single layer system there are three unknown variables: permittivity, conductivity, and the distance the EM wave travels. Fortunately, there are three collected values and independent equations. The three collected values are the direct couple amplitude, rebar reflection amplitude and TWTT. The three equations are velocity as a function of permittivity and conductivity (Equation 4-10), velocity as a function of time and distance, and attenuation (Equation 4-12). Velocity was determined using the direct couple as described in Chapter 7, the distance travelled is determined using Equation 8-1 and attenuation is calculated using Equation 8-2.

$$d_2 = TWTT_2\, v_2 \qquad \textbf{8-1}$$

$$\alpha = \frac{\ln\left(\frac{\emptyset A_{air} d}{A_{bar}} \tau_{12}\tau_{21} \frac{1}{d_2 + 2h_1}\right)}{d_2} \qquad \textbf{8-2}$$

The distance calculated in Equation 8-1 is used to account for the geometric spreading losses as can be seen in the numerator of Equation 8-2 in the form of one over the sum of d_2 and h_1. Once geometric spreading is accounted for, the permittivity and conductivity are calculated by re-arranging the velocity and attenuation equations which are Equations 4-10 and 4-12, respectively. The conductivity contours are then plotted and through the use of a threshold value the repair area is calculated using Surfer® software.

In Chapter 7 it was concluded from laboratory testing that the velocity of an EM wave can be accurately determined using the surface reflection from a GCA. One of the underlying assumptions of Chapter 7 is that the permittivity calculated using the surface reflection is representative of the bulk permittivity. In order to determine if this assumption is valid in the field and if the conductivity can be accurately determined using the surface reflection in conjunction with attenuation, 4 unpaved bridge decks from Nova Scotia were analysed. The method outlined above was compared to the control method developed by Sketchley et al. (2014). Data present by Sketchley et al. was plotted in a similar manner using Surfer®. The control method only used the direct couple to account for variations in transmitted power and employs an optimization process to calculate the permittivity and conductivity.

8.1.1 West River Bridge

The average relative permittivity predicted using the surface reflection was 20, which is significantly outside the typical accepted range for concrete of 4 – 11 (GSSI, 2007). This compares to an average relative permittivity of 9.3 determined using the control method, which is within the accepted range. This difference in results clearly indicates that the relative permittivity predicted using the surface reflection does not represent the bulk permittivity of the structure.

The conductivity predicted using the surface reflection is also significantly higher than the conductivity determined using the control method as can be seen in Figure 8-1. This may be in part due to the high permittivity. The conductivity is calculated using the

attenuation equation, Equation 4-12, which is a function of the real and imaginary component of permittivity. If the attenuation remains constant the conductivity will have to increase with an increase in the real component of permittivity as seen in Figure 8-6. In addition to the variation in the magnitude of the conductivity the visual correlation of the contour plots is low.

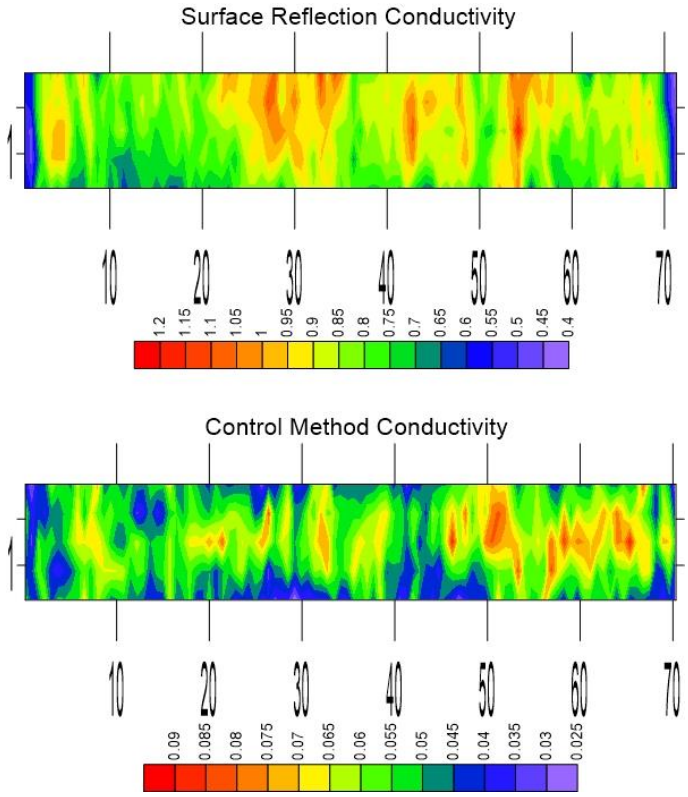

Figure 8-1: Conductivity contours, West River

8.1.2 Milford Bridge

This structure is interesting because there were asphalt patches on the deck which were detected using the permittivity contours created from the surface reflections. The asphalt patches show up as blue/purple in Figure 8-2 and have a relative permittivity of approximately 10 which is on the high end for asphalt which has a typical range of 2 – 12 (Daniels, 2004). The average relative permittivity of concrete determined using the

surface reflection is higher than expected at 23. The average relative permittivity determined by the control method is 8.96 which is within the acceptable range for concrete. Again this clearly indicates that the permittivity calculated using the surface reflection does not represent the bulk permittivity.

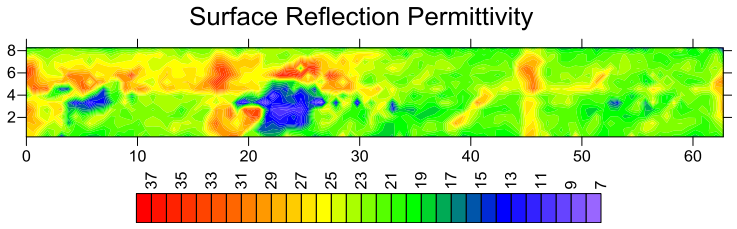

Figure 8-2: Permittivity contours, Milford

The conductivity contour plots in Figure 8-3 appear to have a weak visual correlation. The values of conductivity predicted using the surface reflections again varied significantly from the control method. This may be in part due to the high permittivity values. When comparing the repair areas a threshold value of 1.7 S/m was used for the surface reflection method and resulted in an estimated repair area of 50 m^2. This is 10 m^2 less than the area estimated using the control method which was 60 m^2, using a proprietary threshold value.

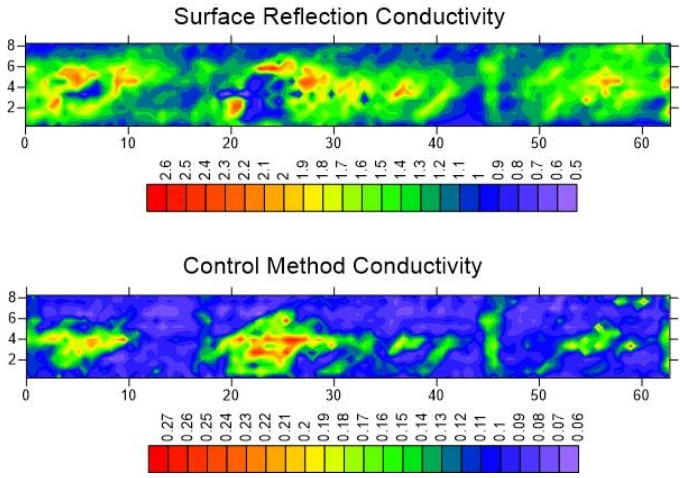

Figure 8-3: Conductivity contours, Milford

8.1.3 Shubenacadie Bridge

Shubenacadie produced the best visual correlation for conductivity as can be seen in Figure 8-4. An issue arose when trying to predict the repair area because, even though they appear to have similar contours, the calculated areas are significantly different. The estimated repair area when using the surface reflections and a threshold value of 1.2 S/m is 20 m^2. The estimated repair area for the control method is 94 m^2. The difference between the two estimated areas is only 11.2% of the total deck area but the cost difference is an estimated $74,000 (Alberta Transportation, 2013).

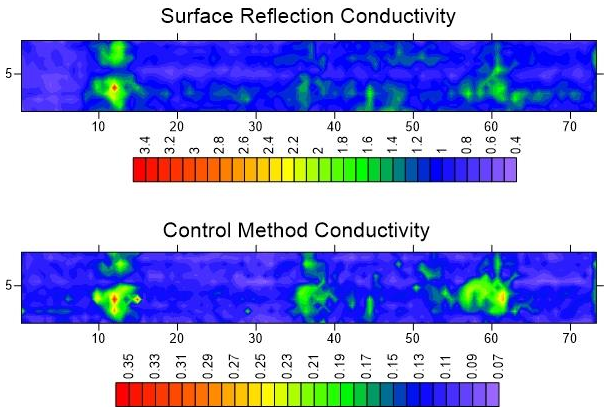

Figure 8-4: Conductivity contours, Shubenacadie

The conductivity values calculated using the surface reflections are an order of magnitude higher than the control method. The high conductivity again may be due to high relative permittivity which was an average of 19.5 for the surface reflection method compared to 11.17 for the control method. This clearly indicated the permittivity calculated using the surface reflection does not represent the bulk permittivity.

8.1.4 Sambro Bridge

The contour plots in Figure 8-5 have a weak visual correlation but produce the best match for estimated repair area. The surface reflection method predicted a repair area of 93 m^2 for a threshold value of 0.85 S/m and the control method estimated a repair

area of 85 m^2. The average relative permittivity calculated using the surface reflections is 16.72 which is higher than the relative permittivity of the control which is 7.36. The average relative permittivity predicted using the surface reflection is the most reasonable so far but still does not agrees with the control method. In addition the conductivity values of the two methods do not compare in magnitude which again could be due to the high permittivity. The results for this structure again clearly indicate the permittivity calculated using the surface reflection does not represent the bulk permittivity.

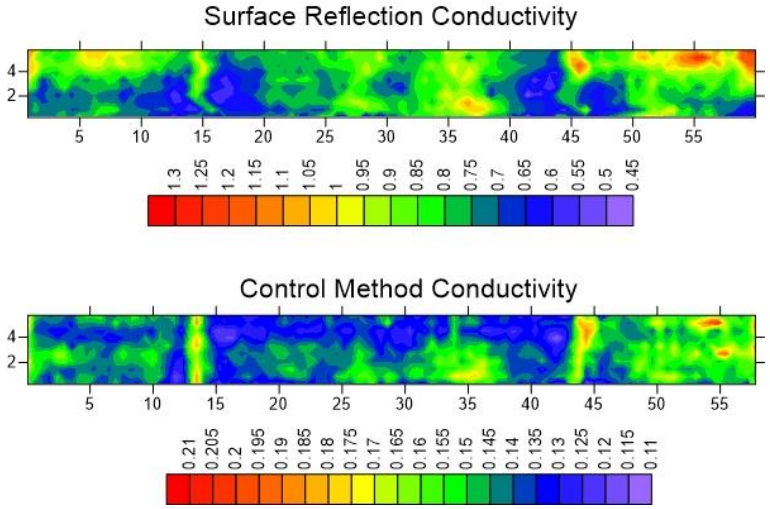

Figure 8-5: Conductivity contours, Sambro

8.2 Discussion

In summary, the permittivity predicted using the surface reflection, permittivity at the surface, does not represent the bulk permittivity for concrete, indicating the method outlined in Chapter 7 is not valid in the field for concrete. The variation in permittivity between the laboratory and the field can be explained due to a decrease in the amplitude of the direct couple which indicates an increase in the amplitude of the surface reflection. The increase in the amplitude of the surface reflection is most likely the result of an increase in the permittivity at the surface which would be caused by a buildup of salt and moisture.

The conductivity values predicted using the surface reflection are significantly outside the typical range associated with concrete which is 1 – 500 mS/m (Abo El-Enein et al., 1995). The high permittivity may result in high conductivity. If attenuation is assumed to remain constant it was shown using Equation 4-12 that any increase in the real component of permittivity will result in an increase in conductivity as can be seen in Figure 8-6. It was also noticed that if the permittivity values of the concrete were assumed constant and within an acceptable range the calculated conductivity was also within an acceptable range; this eliminates the calculation of attenuation as the source of error.

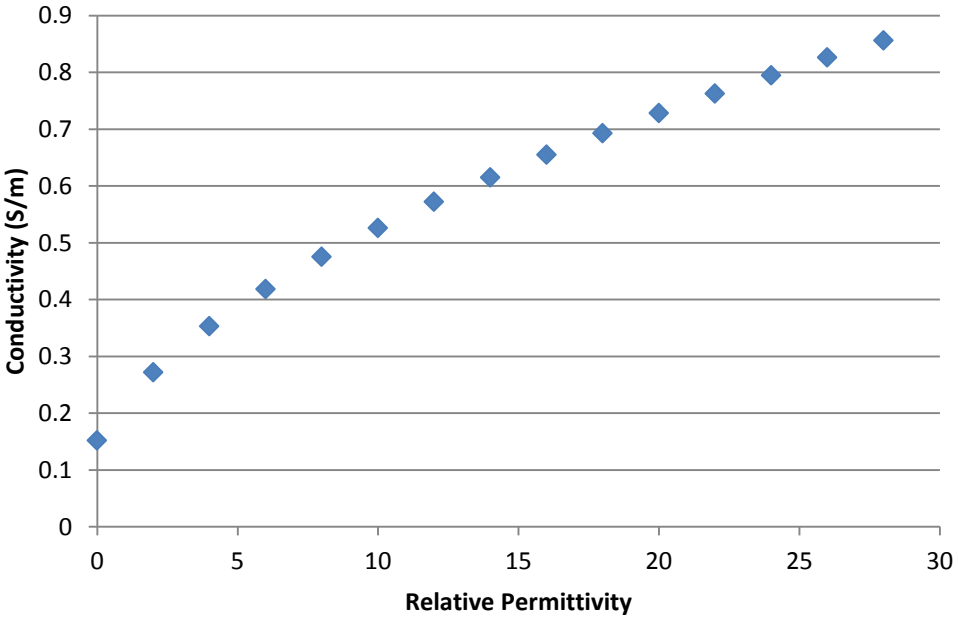

Figure 8-6: Effect of increasing permittivity on conductivity with constant attenuation

The asphalt patches produced a more reasonable permittivity, indicating that the surface reflection method has the possibility of being used on asphalt overlaid decks. More research is required to confirm that the permittivity of asphalt can accurately be determined using the surface reflection from a GCA. The next step should be to survey a road with an air and ground coupled antenna simultaneously so the permittivity values

can be compared. Cores should also be taken to compare the surface reflection permittivity to the bulk permittivity.

Chapter 9 Multilayer

Multilayer systems consist of at least three layers including the layer the antenna is in. For bridges multilayer systems most commonly take the form of concrete decks overlaid with asphalt. The method developed in Chapter 7 and the results in Chapter 8 suggest that a single GCA can be used to determine the permittivity of the top layer allowing GCA to replace air coupled antenna. This in itself is an improvement to the existing methods because GCA's have higher resolution than air coupled due to the smaller radar "footprint". Two semi-conductive and three conductive approaches using the method outlined in Chapter 7 will be developed and discussed.

9.1 Theory

Figure 9-1 shows the ray paths of an EM pulse in a multilayer system. The top most wave which goes directly between the transmitter and receiver is called the direct wave. The wave directly below it is called the surface reflection. The reflected portion of this wave undergoes a 180 degree phase shift because the permittivity of air is less than the permittivity of asphalt, as can be seen in Equation 4-4. The wave below the surface reflection provides information about the asphalt/concrete interface and will be referred to as the interface reflection, A_m. When this wave enters the asphalt the reflected portion undergoes a 180 degree phase shift but the transmitted portion does not. At the asphalt/concrete interface this wave will undergo a 180 phase shift if the permittivity of the asphalt is less than the permittivity of concrete. The final wave is the rebar reflection and in theory undergoes a 180 degree phase shift when it reflects off the rebar because the permittivity of concrete is less than the permittivity of the rebar.

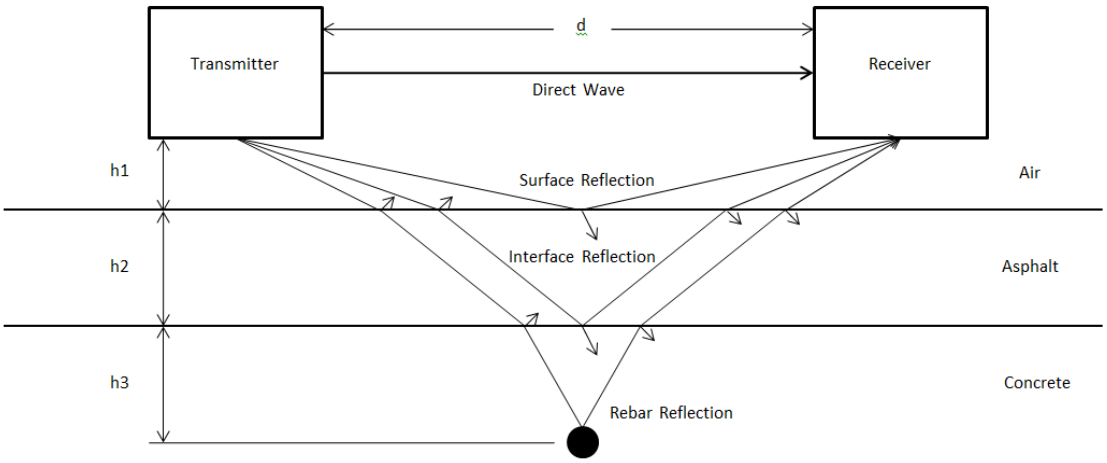

Figure 9-1: Ray path for multilayer ground couple GPR antenna

As the waves travel along their respective ray paths their amplitudes will be reduced and this reduction in amplitude can provide information about the materials the wave interacted with. The reduction or loss in amplitude will be caused by geometric spreading, partial reflection, and attenuation. Geometric spreading does not provide useful information but is easily removed if the distance the wave has travelled is known. The reflection coefficient can be used to determine permittivity and attenuation is used to determine conductivity. Not all the ray paths will experience each type of loss. The amplitude of the direct wave is only affected by geometric spreading. The surface reflection wave experiences losses due to geometric spreading and reflection. The interface reflection wave experiences losses due to geometric spreading, reflections at the surface and interface as well as attenuation in the asphalt. The rebar reflection wave will experience losses due to geometrics spreading, reflection at the surface and interface as well as attenuation in the concrete and asphalt. One of the differences between the models proposed is whether the attenuation occurs in the asphalt or concrete at sufficiently significant levels to be included in the model.

9.2 Semi-Conductive Analysis

A semi-conductive analysis consists of treating only one of the layers as a conductive medium. This section will outline the two possible cases: one where the asphalt is conductive and other where the concrete is conductive.

9.2.1 Concrete Conductive

This method calculates the conductivity of concrete at all location where the GPR data has been collected on the deck; it assumes that the asphalt is a non-conductive, lossless material. A number of papers have had success in calculating permittivity and depth assuming asphalt is lossless, but these papers mostly dealt with roads (Al-Qadi & Lahouar, 2005;Lahouar & Al-Qadi, 2008;Loizos & Plati, 2006;Maser, 1994).

Losses due to geometric spreading are calculated by taking the reciprocal of the distance determined using Equation 7-1 and the reflection losses are calculated using Equations 9-1 and 9-2. The attenuation is calculated using a rearranged Equation 9-4.

$$\tau_{loss} = \tau_{12}\tau_{21} = 1 - r^2 \quad \textbf{9-1}$$

$$r = \frac{\frac{1}{v_2} - \frac{1}{v_3}}{\frac{1}{v_2} + \frac{1}{v_3}} \quad \textbf{9-2}$$

$$A_m = \frac{A_0}{2h_1 + twtt_2 v_2} \tau_{12}\, r\, \tau_{21} \quad \textbf{9-3}$$

$$A_{bar} = \frac{A_0}{2h_1 + twtt_2 v_2 + twtt_3 v_3} \tau_{12}\tau_{23}\, \tau_{32}\tau_{21} e^{-\alpha_3 twtt_3 v_3} \quad \textbf{9-4}$$

A_0 = Amplitude of the wave at the source

Once the attenuation is calculated it can be used in conjunction with the velocity of the EM wave in concrete to determine the conductivity and permittivity of the concrete. The conductivity is then plotted on a contour map to determine repair area.

This method is one of the top contenders for use of GPR in the field; it is relatively simple and the literature indicates that it may be the most reasonable, as accurate results were obtained by others (Maser 1994; Chung et. al., 1992; Alongi et. al., 1992). A modification may need to be made when determining the permittivity and conductivity of the concrete because it is unclear how well the interface reflection can predict the bulk permittivity of the concrete. If it is determined that the interface reflection is a poor predictor of permittivity the rebar amplitude will be corrected for geometric spreading and reflection. Signs of a poor permittivity predictor would include unreasonable permittivity/conductivity values, poor contour correlation between GPR and half cell and a poor correlation between GPR and chain drag results. Then the control method developed by Sketchley et al. (2014) will be used to determine the permittivity and conductivity of the concrete.

9.2.2 Asphalt Conductivity

This method assumes that the asphalt is conductive and, if Chapter 8 is any indication, this approach will produce inaccurate results. This method uses the ratio of the rebar and interface amplitudes to calculate the velocity of the EM wave in the concrete as can be seen in Equation 9-8. The interface amplitude is then used to calculate the attenuation of the EM wave in the asphalt using Equation 9-5.

$$A_m = \frac{A_0}{2h_1 + twtt_2v_2}\tau_{12}\, r\, \tau_{21} e^{-\alpha_2 twtt_2 v_2} \qquad \textbf{9-5}$$

$$A_{bar} = A_0 \frac{(2h_1 + twtt_2v_2 + twtt_3v_3)}{(\tau_{12}\tau_{23}\tau_{32}\tau_{21})} e^{-\alpha_2 twtt_2 v_2} \qquad \textbf{9-6}$$

$$\frac{A_{bar}}{A_m} = \frac{2h_1 + twtt_2v_2}{2h_1 + twtt_2v_2 + twtt_3v_3}\frac{\tau_{23}\tau_{32}}{r} \qquad \textbf{9-7}$$

$$\frac{A_{bar}}{A_m}\frac{2h_1 + twtt_2v_2 + twtt_3v_3}{2h_1 + twtt_2v_2} = \frac{(1-r^2)}{r} \quad \textbf{9-8}$$

When calculating the velocity of the EM waves in concrete an iterative process is used. The iterative process consists of assuming a velocity of the EM wave in concrete, calculating the reflection coefficient and then minimizes the difference between the right and left hand side of Equation 9-8. Once the velocity of the EM wave in concrete is known for a given waveform the attenuation in asphalt is calculated by rearranging Equation 9-5. Then the permittivity and conductivity are calculated using Equations 4-10 and 4-12. Final the rebar amplitude is calculated using Equation 9-6. This method only gives information for the asphalt layer which was unexpected and is not the goal of this research. The reason that this method is only providing information on the asphalt is because any loss in amplitude in the concrete due to attenuation is incorporated into the geometric spreading or interface reflection through the velocity of the EM wave in concrete. When testing this method the corrected amplitude of the rebar, calculated using Equation 9-6, was constant between bars and files. Further investigation revealed the resulting rebar amplitude was equal to the emitted amplitude calculated using Equation 9-9. This indicates that all losses are accounted for and since attenuation in concrete was not one of them the concrete is "truly" a lossless material. This is unreasonable since the literature suggests that concrete needs to be treated as a conductive medium (Alongi et al., 1994;Chung et al., 1994;Lahouar, 2003). Whether this method can be used to determine the conductivity and permittivity in asphalt has yet to be proven and should be researched further.

$$A_0 = \emptyset A_{air} d \quad \textbf{9-9}$$

9.3 Conductive Analysis

In conductive multilayer systems, specifically two layer systems, there are 6 unknowns: conductivity, permittivity and distance travel for each layer. A problem arises because there are only 5 collected pieces of data: surface reflection, interface reflection, rebar reflection and the TWTT for each layer. There are 6 independent equations that can be used: velocity as a function of permittivity and conductivity, velocity as a function of time and distance, and attenuation for each layer. The surface reflection is used to calculate the velocity of the EM wave in asphalt, the interface reflection is used to calculate the velocity of the EM wave in concrete, the rebar reflection is used to calculate the attenuation in the concrete and the TWTT is used to determine the distance travelled. This leaves only the attenuation of asphalt to be determined. So the question becomes how to determine the attenuation of the asphalt? Two solutions will be looked at with the first trying to increase the number of input variables, and the second uses an optimization in effect increasing the number of equations.

9.3.1 Bottom Reflection

This method increases the number of input variables by including the reflection from the bottom of the deck. The velocity of the EM wave in asphalt is calculated using the surface reflection. The reflection at the asphalt concrete interface will be used to calculate the attenuation in the asphalt. The concrete attenuation is calculated using the amplitude of the rebar and the bottom reflection, A_{bttm}, is used to calculate the velocity of the EM wave in concrete. The bottom reflection can be used to calculate the velocity because the velocity of an EM wave in air can be assumed to be 300 mm/ns or if over steel the reflection coefficient can be assumed to be one, provided the entire radar "footprint" reflects off the steel. Once the velocity and attenuation have been calculated Equations 4-10 and 4-12 are used to calculate the permittivity and conductivity of the asphalt and concrete.

$$A_m = \frac{A_0}{2h_1 + twtt_2 v_2} \tau_{12}\, r\, \tau_{21} e^{-\alpha_2 twtt_2 v_2} \quad \textbf{9-10}$$

$$A_{bar} = \frac{A_0}{2h_1 + twtt_2 v_2 + twtt_3 v_3} \tau_{12}\tau_{23}\, \tau_{32}\tau_{21} e^{-\alpha_2 twtt_2 v_2} e^{-\alpha_3 twtt_3 v_3} \quad \textbf{9-11}$$

$$A_{bttm} = \frac{A_0}{2h_1 + twtt_2 v_2 + twtt_3 v_3} \tau_{12}\tau_{23} r\, \tau_{32}\tau_{21} e^{-\alpha_2 twtt_2 v_2} e^{-\alpha_3 twtt_3 v_3} \quad \textbf{9-12}$$

Currently this method cannot be used because the bottom reflection is not reliably detectable due to limitations of the commercially available equipment. If the equipment was able to emit a stronger signal then this method might be able to use individual scans to determine permittivity and conductivity. If this is done other issues that may arise include reflection interference from transverse and longitudinal rebar, studs, and post tensioning cable among others.

9.3.2 Percentile Method

This process is being used successfully for signal layer systems (Barnes et al., 2008). The first step is to plot the amplitude, in decibels, against the TWTT. Next the 90th percentile of the plotted data is determined and used to normalize the remaining data effectively removing losses due to geometric spreading. The 90th percentile is used because it represents concrete which should be relatively uncontaminated with chloride while ignoring the effects of outliers and the only loss should be geometric spreading. Once the data is normalized the main cause of amplitude variation is attenuation and a threshold value can be used to determine deteriorated areas. The control method developed by Sketchley et al. (2014) improved upon this method and calculates conductivity for each point.

When dealing with multilayer systems two plots are evaluated, the interface amplitude vs. TWTT and rebar amplitude vs. TWTT. The 90th percentile of each plot is determined

and these values are fitted to a model that accounts for geometric spreading, reflection and attenuation uses the conductivity of asphalt or the velocity of the EM wave in concrete to minimize the absolute error between the model calculated amplitude and the plot determined amplitude. The model uses the first 90th percentile point and the manipulated variable to calculate the attenuation of the concrete and asphalt. The manipulated variable is either the conductivity of the asphalt or the velocity of the EM wave in concrete which is first estimated and refined with each iteration. Once the attenuation is calculated it is used in conjunction with the remaining 90th percentile TWTT's to determine the amplitude of the rebar and interface reflection. The manipulated variable is varied until the absolute difference between the calculated and recorded rebar amplitudes and interface amplitudes are minimized. The basic formulas used in the program are:

$$A_m = \frac{A_0}{2h_1 + twtt_2 v_2} \tau_{12}\, r\, \tau_{21} e^{-\alpha_2 twtt_2 v_2} \qquad \textbf{9-13}$$

$$A_{bar} = \frac{A_0}{2h_1 + twtt_2 v_2 + twtt_3 v_3} \tau_{12}\tau_{23}\, \tau_{32}\tau_{21} e^{-\alpha_2 twtt_2 v_2} e^{-\alpha_3 twtt_3 v_3} \qquad \textbf{9-14}$$

The velocity of the EM wave in asphalt is determined using the surface reflection method developed in Chapter 7. The asphalt permittivity is calculated by rearranging Equation 4-10 and then used to calculate the attenuation in asphalt, Equation 4-12. The velocity of the EM wave in concrete is determined using Equation 9-13 and attenuation is calculated using Equation 9-14. The conductivity and permittivity of concrete are calculated using Equations 4-10 and 4-12.

Since the velocity of the EM wave in asphalt is calculated using the surface reflection, which in turn is used to calculate the geometric spreading, the plots are not required to remove the effects of geometric spreading. Even if the surface reflection could be used to calculate something besides geometric spreading the same assumptions cannot be made for a multilayer system as can be made a single layer system. In a single layer

system, for a given TWTT and assuming constant permittivity, any loss in signal is due to attenuation but in a multilayer system it is possible to have significant attenuation in the asphalt and a strong reflection at the interface causing "bad" asphalt to appear as "good". This indicates the amplitude of the EM wave is affected by both attenuation and the interface reflection which means the 90th percentile cannot be used to indicate "good" or "bad" material. In addition this method assumes that "good" asphalt corresponds to "good" concrete which is not true, as seen in Figure 9-2, so the two plots cannot be compared. The blue circles in Figure 9-2 are the amplitudes that are greater than or equal to the 90th percentile for the interface reflection vs. TWTT plot. It is not surprising that this is the case because Maser (1991) used high interface reflection as an indication of deteriorated concrete not clean concrete. In the end this method cannot be used in its current form to determine conductivity and permittivity for the concrete and asphalt.

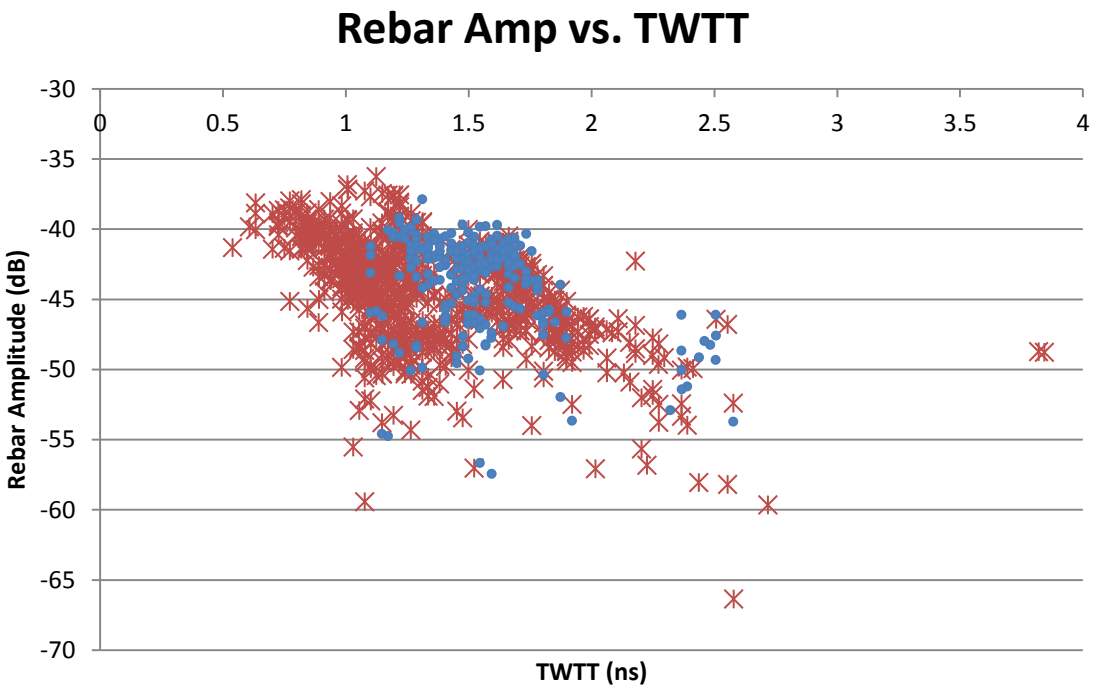

Figure 9-2: 90th percentile data of the interface amplitude vs. TWTT plotted on the rebar amplitude vs. TWTT plot

9.3.3 Constant Concrete Velocity

In this method the velocity of the EM wave in concrete is assumed to be constant; it is adjusted until the permittivity of the asphalt is minimized. It should be noted that the change in asphalt permittivity achieved through this minimization was small on the order of 0.02 permittivity units yet the result variation in concrete was close to 10 mm/ns. There is no justification for minimizing the asphalt permittivity. It was noticed that there was a minimum value in the range of velocities of interest, and the asphalt permittivity's were reasonable, so instead of randomly guessing a velocity of the EM wave in concrete this seemed to be a better solution.

This method uses Equation 9-13 to calculate the attenuation of asphalt. The velocity of the EM wave in asphalt is determined using the procedure developed in Chapter 7. The velocity of the EM wave in concrete is determined by minimizing the permittivity of asphalt and the attenuation is determined using Equation 9-14. The conductivity and permittivity of asphalt and concrete are determined using Equations 4-10 and 4-12.

This method may produce erroneous permittivity and conductivity values for concrete because the velocity of the EM wave in concrete is assumed to be constant. The permittivity of the concrete can easily vary across the entire deck due to differences in moisture content.

9.4 Results and Discussion

Only two of the proposed methods were evaluated, the semi-conductive method that assumes the asphalt is non-conductive and the fully conductive method that assumes the velocity of concrete is constant. A reasonable range of permittivity of asphalt is 2 – 12 (Daniels, 2004) and concrete is 4 - 11 (Jol, 2008). The reasonable range of conductivity in concrete and asphalt is 0 – 0.5 S/m (Abo El-Enein et al., 1995).

9.4.1 Musquodoboit Bridge

As can be seen in Table 9-1 the permittivity and conductivity are within a "reasonable" range, with the exception of some of the maximum values. The maximum expected conductivity for concrete is approximately 0.5 S/m which is significantly lower than the calculated maximums. The maximum permittivity of concrete, Perm_c, in the semi-conductive model and maximum permittivity of asphalt, Perm_a, in both models is high.

	Semi-Conductivity			Conductivity			
	Perm_a	Perm_c	Cond_c (S/m)	Perm_a	Cond_a (S/m)	Perm_c	Cond_c (S/m)
Average	4.673	7.813	0.325	4.635	0.057	11.163	0.390
Min	1.574	2.110	0.084	1.555	0.001	8.135	0.023
Max	15.456	29.923	1.541	15.786	0.699	11.684	1.138

Table 9-1: Permittivity and conductivity, Musquodoboit

The high permittivity was most likely caused by wet conditions before and during testing. The high conductivity of asphalt, Cond_a, and concrete, Cond_c, may be compensating for the high permittivity as mentioned in Chapter 8 and can be seen in Figure 8-6. Figure 9-3 agrees with this because after a permittivity of about 9 the conductivity and permittivity seem to have a stronger correlation. When considering permittivity values less than 9 there are only 6 points where the conductivity is greater than 0.5 S/m out of a total of 828 points or 0.7% of the points.

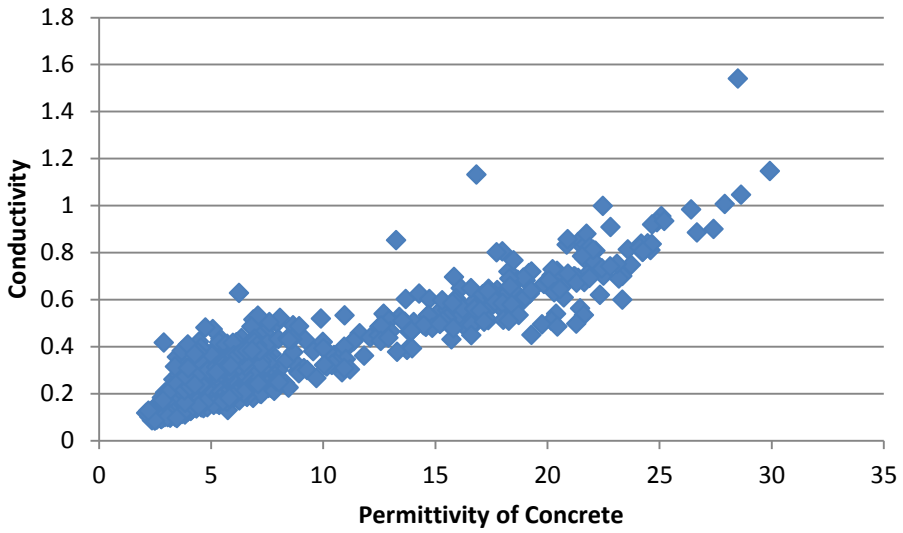

Figure 9-3: Permittivity of concrete vs. conductivity of concrete, semi-conductive model Musquodoboit

A similar situation can be seen in Figure 9-4 where after a relative permittivity of 6 the conductivity and permittivity seem to be related. The conductivity values in Figure 9-4 may not represent the actual conductivity in the concrete because the velocity of the EM wave in concrete was assumed constant.

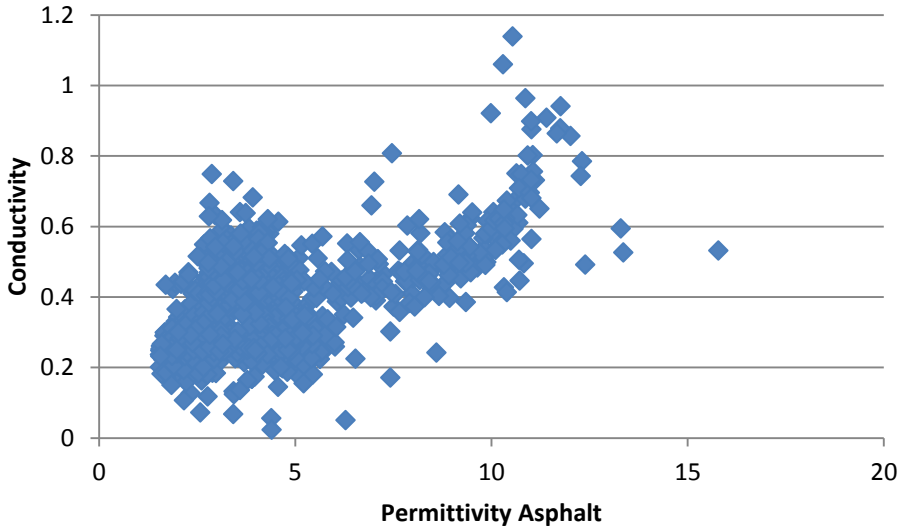

Figure 9-4: Asphalt permittivity vs. conductivity, conductive model Musquodoboit

The minimum asphalt permittivity for the semi-conductive model may be due to debris at the surface or the antenna lifting off the ground. The low concrete permittivity can be explained by the low permittivity of the asphalt. The concrete permittivity is based on the reflection coefficient with is dependent on the difference in permittivity between the asphalt and concrete. This means any error in estimating the asphalt permittivity will result in an error when calculating the concrete permittivity. The relationship between the concrete and asphalt permittivity can clearly be seen in Figure 9-5.

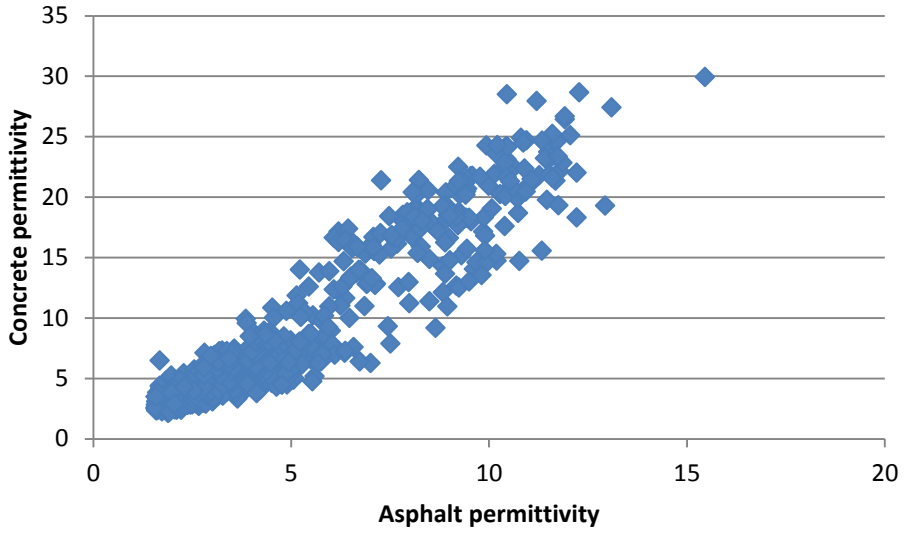

Figure 9-5: Concrete and asphalt permittivity, semi-conductive model Musquodoboit

The asphalt permittivity values and contours are for all intents and purposes identical between the conductive and semi-conductive models as can be seen in Figure 9-6 and Table 9-1. This is not surprising since they are calculated in the same manner. The higher permittivity near the curbs is somewhat expected since most if not all bridges have some sort of cross slope which forces water and debris to collected at the curb/curbs. The debris itself may be wet and/or moisture may accumulate in the asphalt near the curbs.

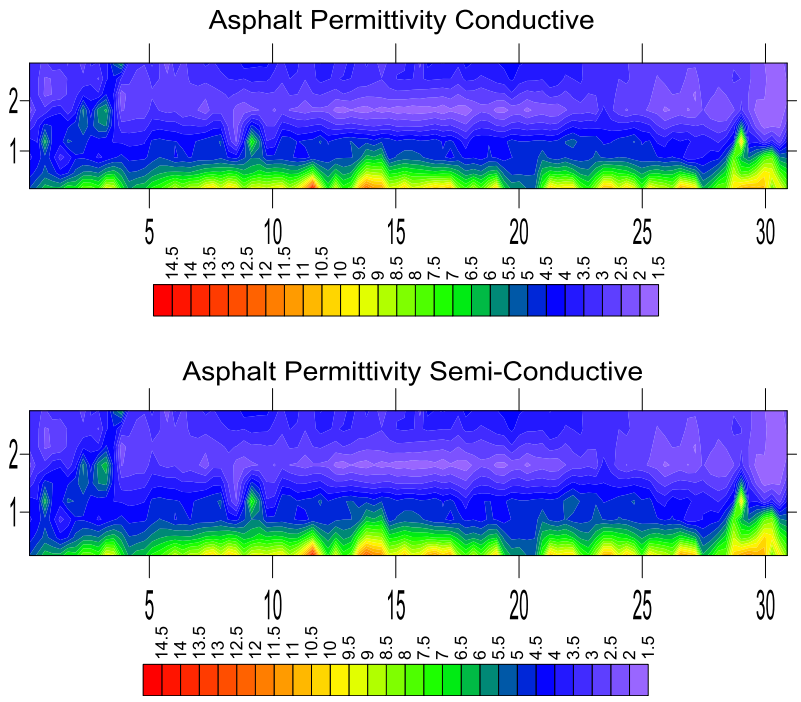

Figure 9-6: Permittivity of asphalt, Musquodoboit

Figure 9-7 shows the concrete permittivity for the semi-conductive model. When compared to the asphalt permittivity contour map it can be seen that they have similar contours. This would indicate that wet areas at the asphalt surface correspond to wet areas at the concrete surface which is not surprising.

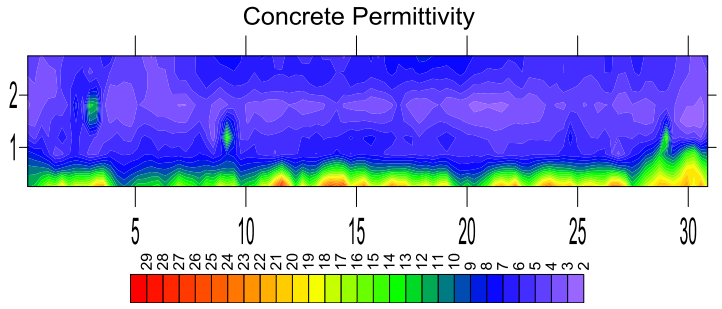

Figure 9-7: Concrete permittivity, semi-conductive model Musquodoboit

The asphalt conductivity is low except for a few locations that occur at the edge which correspond to areas of high asphalt permittivity. In Figure 9-8 it can be seen that the

overall conductivity of asphalt is low and it may be reasonable to assume that asphalt is non-conductive.

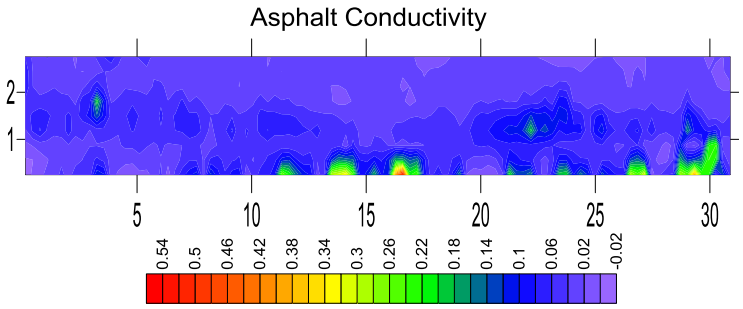

Figure 9-8: Asphalt conductivity, Musquodoboit

The concrete conductivity contour maps have a similar range of values and contours but there is enough discrepancy between the conductive and semi-conductive analysis to say they are not the same. It can be seen in Figure 9-9 that the conductive model is indicating more deterioration than the semi-conductive model. This could be due to the fact the velocity of the EM wave in concrete is assumed to be constant resulting in errors when calculating conductivity.

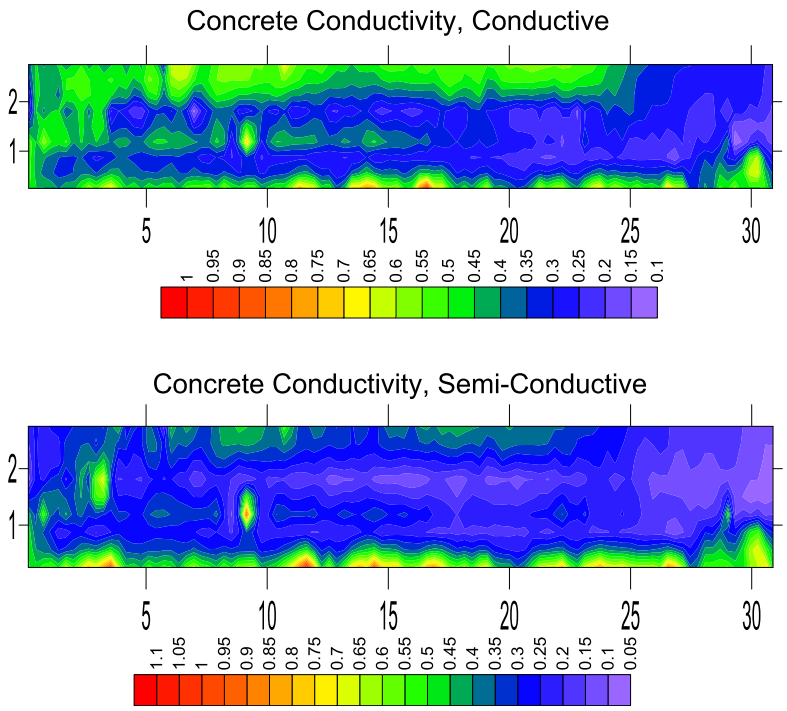

Figure 9-9: Concrete conductivity, Musquodoboit

9.4.2 Shediac Bridge

The only reasonable value obtained from this structure is the permittivity of asphalt, Perm_a, calculated using the semi-conductive model. There are a few spots of low permittivity which could be due to the antenna being lifted off the surface or debris.

	Semi-Conductive			Conductive			
	Perm_a	Perm_c	Cond_c (S/m)	Perm_a	Cond_a (S/m)	Perm_c	Cond_c (S/m)
Average	5.482	-114.865	3.410	5.275	0.149	-159.884	3.469
Min	1.114	-6837.907	0.158	-8.209	0.000	-	0.084
Max	11.648	15.284	56.278	13.923	1.796	205.548	60.467

Table 9-2: Permittivity and conductivity, Shediac

The permittivity and conductivity of concrete, Perm_c and Cond_c, respectively, have very erroneous result. When the permittivity or conductivity of concrete is plotted

against the TWTT the data become more erroneous as the TWTT approaches zero as seen in Figure 9-10. This applies to both the conductive and semi-conductive models.

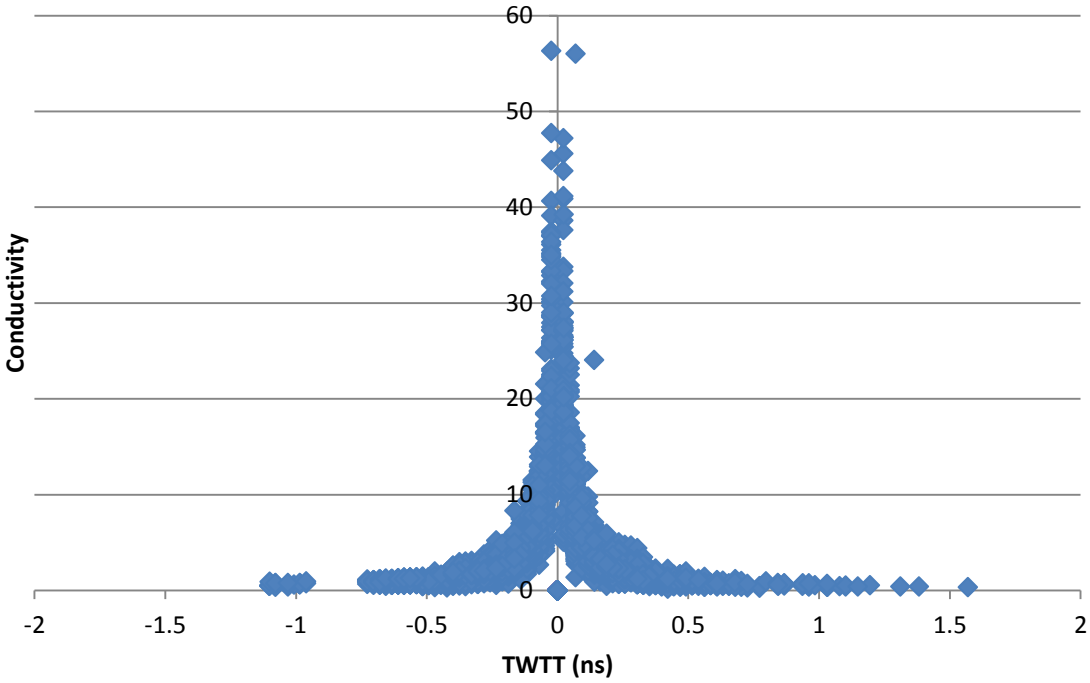

Figure 9-10: Error in conductivity due to TWTT, Shediac

It appears the asphalt layer is thin and there is little cover on the rebar resulting in interference between the reflections. Figure 9-11 shows how the rebar amplitude is interfering with the direct couple with no indication of asphalt.

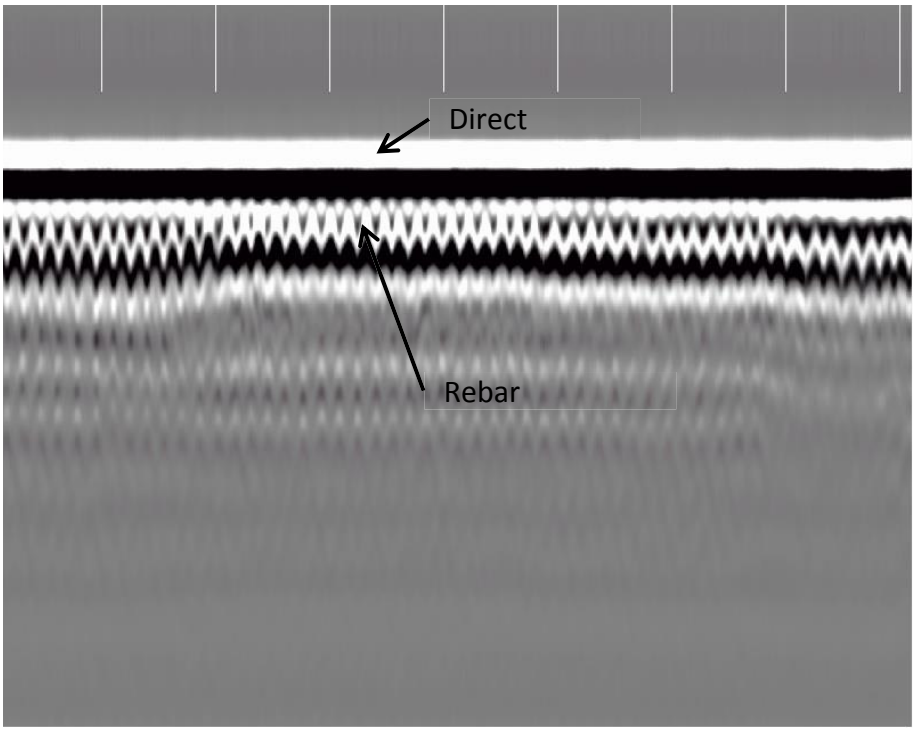

Figure 9-11: Rebar reflection interference with direct couple

The permittivity of the asphalt calculated using the two methods produces similar contours and values which can be seen in Figure 9-12. Again this is expected since the same procedure was used to calculate the permittivity of both methods.

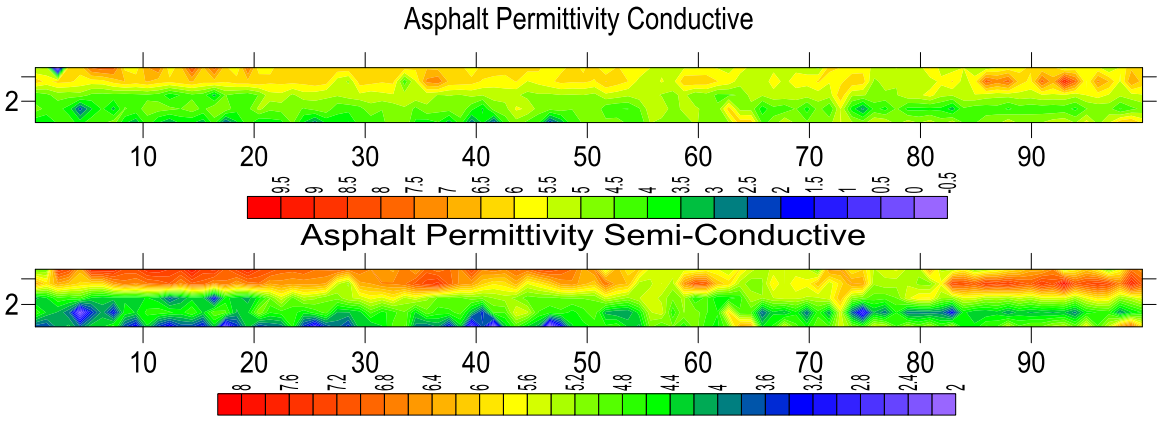

Figure 9-12: Asphalt permittivity, Shediac

In Figure 9-13 it can be seen that majority of the conductivity is low. In fact 61% of the deck has conductivity values below 0.1 S/m and 81% is below 0.2 S/m. Due to the low conductivity and the simplicity of the math, the semi-conductive model should be researched further as a viable option for evaluating the condition of reinforced concrete decks.

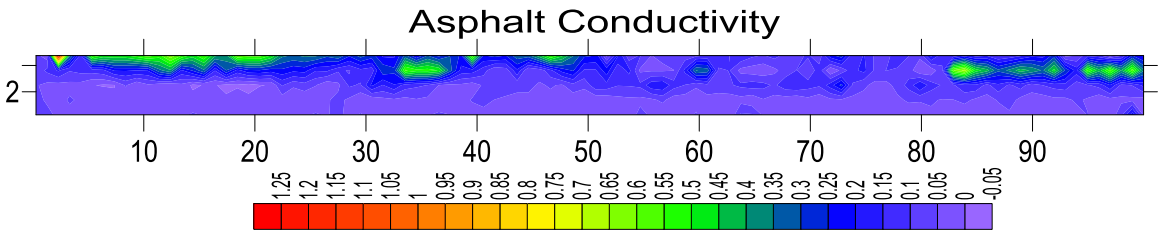

Figure 9-13: Asphalt conductivity, Shediac

From Figure 9-14 it can be seen that both methods produce very similar contours and conductivity values for concrete. It appears that the method used has little effect on the results for this structure.

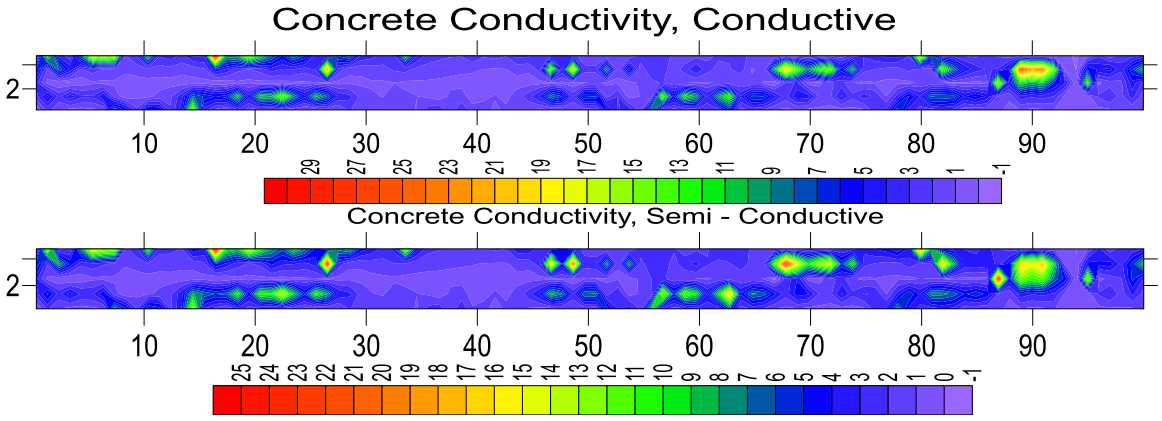

Figure 9-14: Concrete conductivity, Shediac

The half cell results are presented in Figure 9-15 and it can be seen that they do not match the conductivity values presented in Figure 9-14. In fact it turns out that the uncorrected rebar amplitude seen in Figure 9-16 produces more accurate results.

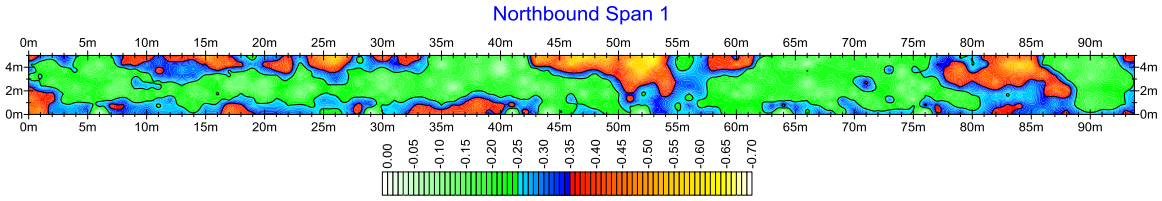

Figure 9-15: Half cell results, Shediac (Barnes)

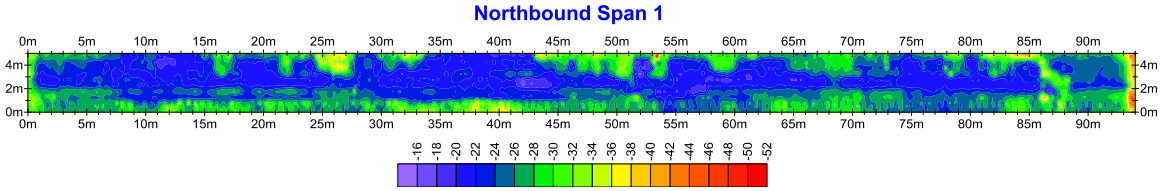

Figure 9-16: Modified uncorrected rebar reflection amplitude, Shediac (Barnes)

9.4.3 Bedford North Bridge

The results for this structure are outside the acceptable range except for the conductivity of asphalt. This structure has a low asphalt permittivity which is most likely due to the low surface reflection. The average permittivity of concrete is low for the semi-conductivity model which may be due to the low asphalt permittivity. The average conductivity of concrete for the semi-conductive model is reasonable but the max value is too high and may be a result of the high concrete permittivity. The asphalt conductivity is reasonable but the concrete permittivity and conductivity for the conductive model are not reasonable.

	Semi-Conductive			Conductive			
	Perm_a	Perm_c	Cond_c (S/m)	Perm_a	Cond_a (S/m)	Perm_c	Cond_c (S/m)
Average	2.112	3.071	0.228	1.935	0.097	61359.886	13006.630
Min	1.127	-	0.051	0.932	0.006	-7.77E+06	2142.298
Max	6.996	232.842	10.659	6.503	0.343	158768.292	165401.197

Table 9-3: Permittivity and conductivity, North Bedford

Extreme permittivity and conductivity values seem to be caused by the short TWTT as seen in Figure 9-17. There are a few points that cannot be explained by the TWTT but they are not going to be investigated because there are only 7 out a total of 2542 points.

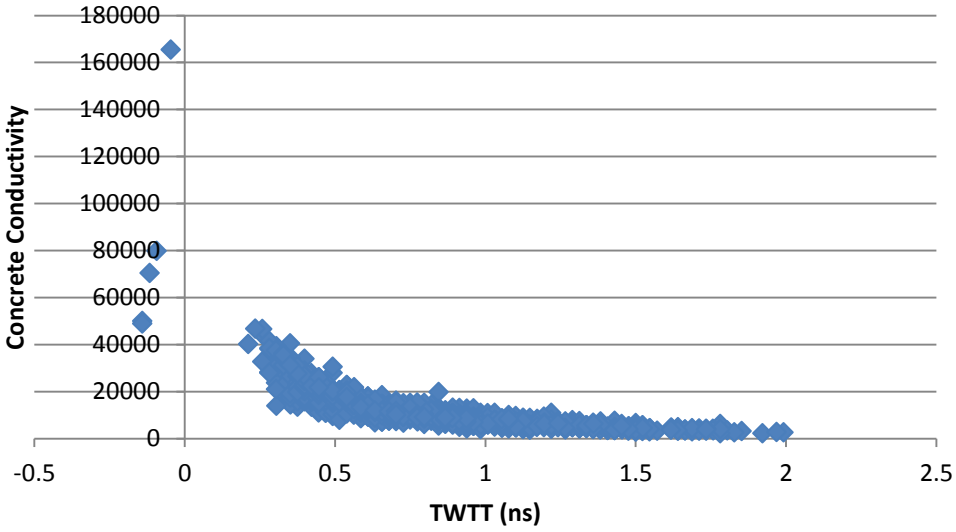

Figure 9-17: Error in conductivity due to TWTT, North Bedford

The permittivity of Shediac asphalt is similar to that of the other two structures already discussed but is lower than expected, Figure 9-18. Almost the entire structure has a permittivity under 4 and in fact the majority of the structure has a permittivity under 3. This can be credited to the higher than normal direct couple indicating a low surface reflection. In general the direct couple is in the range of 2000 – 3000 AU but for this structure it is in the range of 5000 – 6000 AU. The first thought is the gain was not accounted for properly but the removed gain matched the gain Radan indicated, *i.e.* the

wrong gain was using in Equation 7-4. When using the radar the gain can be set during the configuration stage. This gain will apply a permanent amplification to the returning signal which Radan records; this gain is easily removed using Equation 7-4. The radar software also allows the user to choose a configuration type depending on the test; two of the choices are concrete and highway. It was notice that the amplitude of the direct wave would change depending on the configuration type even when the same gain was applied. A test was done, which is outlined in the Appendix, to determine the gain applied by different configuration types that is not recorded by Radan. From this test it was noticed that a concrete configuration type with zero applied gain in fact had a 9.4 dB gain when compared to a zero gain custom configuration type, which was used for the Chapter 7 tests. It is possible that a different configuration type besides concrete was used but there is no way of knowing. Another possibility may be that the asphalt has an abnormally low permittivity.

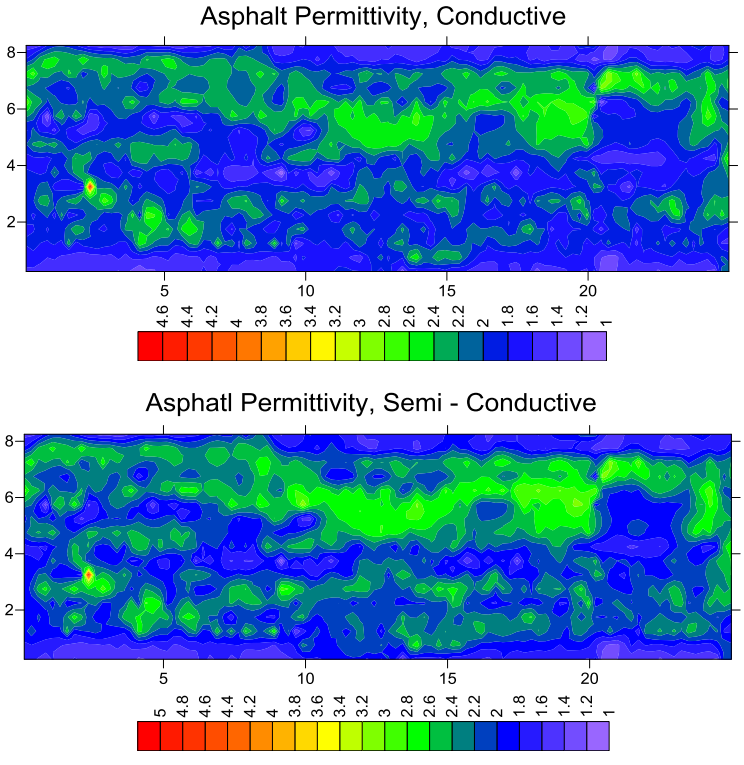

Figure 9-18: Asphalt permittivity, North Bedford

The asphalt conductivity again is low as can be seen in Figure 9-19. Over 99% of the deck area has conductivity values below 0.2 S/m, 95% below 0.15 S/m and 53% below 0.1 S/m.

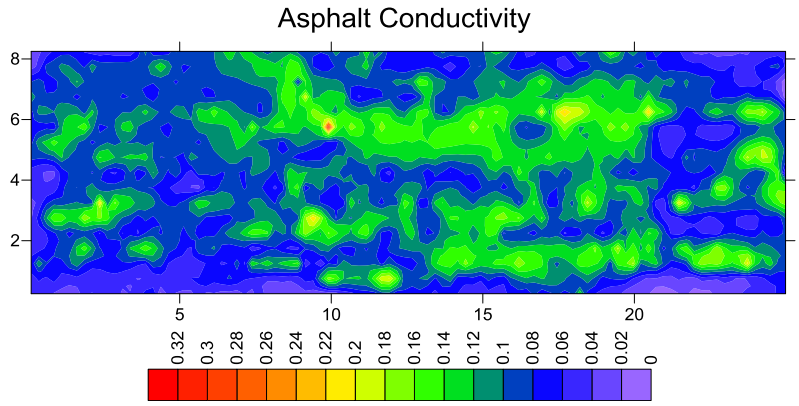

Figure 9-19: Asphalt conductivity, North Bedford

The conductivity and permittivity for concrete are not plotted because there is very little variation and the results are erroneous as can be seen in Figure 9-20.

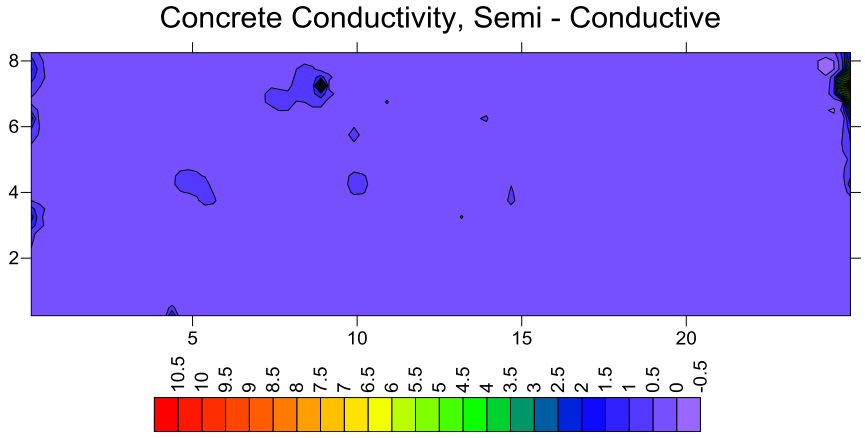

Figure 9-20: Concrete Conductivity, North Bedford

9.4.4 Discussion

The predicted permittivity of asphalt was the “same” regardless of whether the asphalt is assumed to be conductive or not. As stated in each subsection this is not surprising because both the conductive model and semi-conductive model calculate the velocity using the method developed in Chapter 7. In the case of the semi-conductive model the velocity is converted directly to permittivity using Equation 4-11. The conductive model uses the velocity and attenuation to calculate conductivity and permittivity. More importantly the values of permittivity are reasonable for asphalt. There are a few instances where the permittivity is lower than would be expected but this could be caused by the antenna lifting off the ground or debris on the surface. Also some of the maximum values are higher than expected but are in the realm of being feasible if there is moisture at the surface, debris or even concrete patches. The permittivity of asphalt for North Bedford is lower than expected and in this case debris or the antenna lifting off the deck is unlikely because permittivity is low over the entire deck. It was noted that the direct couple had a higher amplitude than normal as stated in section 9.4.3. This higher direct couple may be due to an error in gain correction caused by an unknown configuration type. When the gain correction was done the gain that Radan provided was used and it was assumed that the configuration type was concrete. Since Radan does not provide information on configuration types the author was unable to be confirmed what configuration type was used. It is also possible that the permittivity of the asphalt was low. This could be due to a higher air void content than normal, possibly the type of aggregate or asphalt binder used may have a lower permittivity than normal.

It is also clear from the results that asphalt is generally non-conductive. There are a few areas that have a significant level of conductivity but these appear to have little effect on the predicted conductivity of the concrete. A semi-conductive model that assumes asphalt as non-conductive should be considered because it is significantly easier mathematically than a fully conductive model and appear to provide reasonable results. At the very least the results provided in this chapter has not disproven the usefulness of a semi-conductive model.

There are a number of issues that need to be addressed if GPR is going to be used to assess asphalt overlaid bridge decks. These issues include signal interference, how the interface reflection relates to the bulk properties of the concrete, radar cross section of the rebar and the phase shift of the EM wave as it travels between layers. The signal interference occurs for one of two reasons. First the asphalt layer may not be thick enough to separate the surface reflection from interface reflection. Second there may not be enough cover over the rebar to separate the interface reflection from the rebar reflection. This interference causes a change in the measured amplitude and TWTT of the rebar reflection. Since the radar operation has no control over the rebar cover or asphalt thickness it may be helpful to use a higher frequency antenna such as 2.6 GHz. This will reduce the penetration depth but may produce clear enough results to improve accuracy. As the frequency of an EM wave increases, for the same power output, the penetration depth decreases along with the wavelength. A reduction in wavelength results in a higher resolution which can be seen in Equation 9-15. The minimum thickness that can be detected without interferences is Δd where, T is the period of the wave (Al-Qadi & Lahouar, 2005).

$$\Delta d = \frac{vT}{2\sqrt{\varepsilon_r}} \qquad \textbf{9-15}$$

Multiple asphalt layers can also cause signal interference. On roads it is common to add additional pavement layers throughout its life cycle. These overlays may have different permittivities that result in reflections that are not accounted for in the models and that may interfere with each other. Al-Qadi & Lahouar (2005) have found a way of dealing with reflection interference due to multiple layers of thin asphalt with different permittivities through de-convolution. One of the deconvolution methods identifies strong reflection and uses a least square fittings to estimate the amplitude. The estimated amplitudes are then used to create a theoretical waveform which is removed from the actual waveform to reveal the weaker reflections. This process is repeated

until all the reflections are identified. Deconvolution resulted in an increase in accuracy from 12% to 3% when estimating the thickness of the asphalt using the surface reflection. For bridge structures it is unlikely that additional layers of asphalt would be added at different times because it may require the joints and possibly the barrier heights to be adjusted. However it is not uncommon for the asphalt overlay to consist of a number of lifts that may become separated causing reflections. If de-bonding between asphalt layers occurs it may be possible to use a method similar to the ones used for roads.

Even when there is no signal interference the conductivity and permittivity of concrete produce somewhat erroneous results near the curbs. This could be caused by moist asphalt and a buildup of salt resulting in a high asphalt permittivity and thus a high concrete permittivity. The moisture can build up near the curbs because most bridges have cross slopes that force water to accumulate and flow along the curb. The second possibility is that the interface reflection may produce a permittivity that is not representative of the bulk permittivity of the concrete. This would be similar to the situation occurring when the surface reflection is used to calculate the permittivity of concrete for single layer systems. Water could also pool at the interface or the waterproofing may affect the interface reflection amplitude. In the case of pooling water the permittivity would be overestimated and cause an overestimation in the conductivity as well. This situation is most likely to occur near the curbs, due to the cross slope, which matches the results. A fourth possibility it that the asphalt is de-bonding from the concrete which could be filled with either air or water again causing an error in the estimated bulk permittivity of concrete.

Chapter 10 Discussion, Conclusion, and Recommendations

10.1 Discussion

This thesis focused on using a GCA on asphalt overlaid bridge decks to conduct condition assessments. In order to achieve this goal an accurate model of geometric spreading needed to be confirmed, a procedure for determining the permittivity of the top layer, and a model for a multilayer system needed to be developed. The research presented above addresses each of these goals with varying levels of success.

Chapter 6 outlines a test that was conducted to determine which of the existing geometric models best represented the actual behavior of the wave for the antenna used. From this test it was determined that the amplitude of the signal decreases at a rate of one over the distance except when the direct wave is used as the reference wave; in that case a calibration factor is required. The need for a calibration factor was realized because the slope of the amplitude ratio vs. distance ratio when the direct wave was used at the reference wave was not one. This calibration factor possibly accounts for errors such as using far field equations in the near field, internal reflection, and inaccuracies in the T-R spacing.

Chapter 7 describes a method that enables a GCA to be used to determine the permittivity of the top layer. This method isolated the surface reflection from the direct couple by subtracting the direct wave. Fresnel's equation for reflection is then used to determine the permittivity of the uppermost layer. This method is able to accurately determine the permittivity in the laboratory for both asphalt and concrete. The field test which used bare unpaved bridge decks produced higher than expected permittivity, and conductivity, for the concrete which suggests that this method may not be able to be used in the field on concrete decks. One of the structures in the field had asphalt patches and the permittivity calculated in these areas was within reason for asphalt suggesting that the surface reflection is able to "accurately" predict the permittivity of asphalt in the field.

A number of multilayer models were proposed in Chapter 9 which included two semi-conductive and three fully conductive models. The two semi-conductive model treated one layer as non-conductive and the other layer as conductive. The semi-conductive model that treats the asphalt layers as conductive only provides information about the asphalt. The "corrected" rebar amplitude matches the output signal amplitude indicating all the losses are accounted for and attenuation in concrete was not one of them. The semi-conductive model that treats the concrete as conductive produces conductivity result that are comparable to the ones produced using the fully conductive model. This semi – conductive model is one of the most promising models proposed.

Three conductive models were proposed one of which used the bottom reflection to increase the number of equations. This method is currently not possible because the bottom reflection is not reliably detectable. The 90^{th} percentile method which is an adaptation of a method created by Barnes et al. (2008) has a number of issues, such as assuming the 90^{th} percentile of the interface reflection represents "clean" concrete, and was not used to analysis the data. The third conductive model used to analysis the data assumes that the velocity of the EM wave in concrete is constant. The conductivity values produced in asphalt where low and the conductivity contours for concrete matched the semi-conductive model that assumed non-conductive asphalt. These two facts indicate that the asphalt can be treated as non–conductive or at least has not disproven it.

10.2 Conclusions

There are a number of conclusions that arouse from this research and include:

1. Geometric spreading for a ground coupled antenna can be assumed to be proportional to the inverse of the distance if the direct wave is not the reference wave.
2. The direct wave can be used as a reference amplitude for computing the permittivity of the uppermost layer as long as a calibration factor is used.

3. The velocity of the EM wave can be accurately determined for asphalt and concrete samples in the laboratory using the surface reflection from a ground coupled antenna.
4. The velocity of an EM wave in concrete could not be accurately determined in the field using the surface reflection from a ground coupled antenna.
5. The velocity of an EM wave in asphalt may accurately be determined in the field using the surface reflection from a ground coupled antenna.
6. Asphalt can be treated as a non-conductive medium when determining the conductivity in concrete for asphalt overlaid bridge decks.

10.3 Recommendations

Further research is required before condition assessment can be conducted for multilayer systems using the methods investigated in this research. Areas requiring addition research include; signal interference between layers, the ability of reflections to predict bulk permittivity of concrete and effects of different conditions at the interface on the amplitude of the interface reflection.

The first question that needs to be answered is how well does the method described in Chapter 7 compared to the results obtained from an air coupled antenna. This can easily be done with the SIR 20 due to its dual transmitter capacity. This experiment would entail using both an air and GCA at the same time and calculate the permittivity of the top layer for each antenna. For extra redundancy it would also be beneficial to take cores to compare the permittivity calculated using the surface reflection with the permittivity calculated using the TWTT.

Once it is confirmed that a GCA can replace an air coupled antenna for accurately predicting the permittivity of asphalt the amplitude of the interface reflection needs to be looked at. Two areas regarding the interface reflection need to be looked at. First the rebar and surface reflections often interfere with the interface reflection and second how accurately can the bulk permittivity of the concrete be predicted using the

interface reflection. To address the accuracy of the interface reflection in determining the permittivity of concrete, laboratory testing should be the first step. The first set of laboratory tests should try to predict the permittivity of concrete with an asphalt sample directly on top of the concrete in “dry” conditions. The next step would be to place a waterproof membrane between the asphalt and concrete sample and see if there is any change in the amplitude of the interface reflection. Once the effects of the waterproof membrane are understood another test should be done to see the effects of water pooling at the interface on the interface reflection.

Another issue that may arise is how well the permittivity at the surface of the concrete represents the bulk permittivity. If it is found that the interface reflection does not accurately predict the bulk permittivity of the concrete then the effect of reflection and geometric spreading caused by the asphalt should be removed from the rebar reflection. Then the correct rebar reflection could be analysed using the method developed by Sketchley et al. (2014).

Every structure that was evaluated using the multilayer analysis had some level of interference between layers. The interference problem may be solved with a higher frequency antenna. Currently GSSI has antennas with a central frequency up to 2.6 GHz with a depth range of 0.4 m. If a higher frequency antenna is unable to completely solve the problem a method similar to the one used by Lahouar & Al-Qadi (2007) for thin asphalt should be looked at.

References

Alberta Transportation (2013). *Unit Price Averages Reports*. Retrieved from http://www.transportation.alberta.ca/Content/docType257/Production/UnitPriceList.pdf

Alberta Transportation (2008). *Bridge Inspection and Maintenance System – Inspection Manual*. Retrieved from http://www.transportation.alberta.ca/Content/docType30/Production/BIMMnlv3.1.pdf

Alberta Transportation (2007). *BIM Reference Manual, Bridge inspection and Maintenance System.* Retrieved from http://www.transportation.alberta.ca/2657.htm

Alongi, A. J., Clemena, G. G., & Cady, P. D. (1992). Condition evaluation of concrete bridges relative to reinforcement corrosion, volume 3: method for evaluating the condition of asphalt-covered decks (No. SHRP-S-325).

Al-Qadi, I. L., & Lahouar, S. (2005). Measuring layer thicknesses with GPR–Theory to practice. *Construction and building materials*, *19*(10), 763-772.

Angst, U. (2011). Chloride induced reinforcement corrosion in concrete: Concept of critical chloride content–methods and mechanisms.

Standard, A. S. T. M. (2012). D4580: Standard Practice for Measuring Delaminations in Concrete Bridge Decks by Sounding, ed. *West Conshohocken, PA: ASTM International*.

Standard, A. S. T. M. (2009). C876: Standard Test Method for Corrosion Potentials of Uncoated Reinforcing Steel in Concrete, ed. *West Conshohocken, PA: ASTM International.*

Barnes, C. L. (2008). Evaluating Moisture Damage in Asphalt Concrete Using Surface Waves. PhD Thesis, Dalhousie University.

Barnes, C. L., Trottier, J. F., & Forgeron, D. (2008). Improved concrete bridge deck evaluation using GPR by accounting for signal depth–amplitude effects.*NDT & E International*, *41*(6), 427-433.

Barnes, C. L., & Trottier, J. F. (2004). Effectiveness of ground penetrating radar in predicting deck repair quantities. *Journal of infrastructure systems*, 10(2), 69-76.

Belli, K., Wadia-Fascetti, S., & Rappaport, C. (2008). Model based evaluation of bridge decks using ground penetrating radar. *Computer-Aided Civil and Infrastructure Engineering*, *23*(1), 3-16.

Bertolini, L., Elsener, B., Pedeferri, P., Redaelli, E., & Polder, R. B. (2004).*Corrosion of steel in concrete: prevention, diagnosis, repair*. John Wiley & Sons.

Billington, E. D. (2003). GPR Surveying to Help Determine Condition of a Concrete Bridge Deck. Retrieved from: http://www.dot.state.fl.us/statematerialsoffice/geotechnical/conference/materials/billington.pdf

Broomfield, J. P. (2006). Corrosion of steel in concrete: understanding, investigation and repair. CRC Press.

Callister, W. D., & Rethwisch, D. G. (2012). Fundamentals of materials science and engineering: an integrated approach. John Wiley & Sons.

Chung, T., Carter, C. R., Masliwec, T., & Manning, D. G. (1992). Impulse radar evaluation of asphalt-covered bridge decks. *Aerospace and Electronic Systems, IEEE Transactions* on, 28(1), 125-137.

Chung, T., Carter, C. R., Masliwec, T., & Manning, D. G. (1994). Impulse radar evaluation of concrete, asphalt and waterproofing membrane. *Aerospace and Electronic Systems, IEEE Transactions* on, 30(2), 404-415.

Clemeña, G. G. (1983). Nondestructive inspection of overlaid bridge decks with ground-penetrating radar. *Transportation Research Record*, (899).

Daniels, D. J. (Ed.). (2004). *Ground penetrating radar* (Vol. 1). Iet.

El-Enein, S. A., Kotkata, M. F., Hanna, G. B., Saad, M., & El Razek, M. M. (1995). Electrical conductivity of concrete containing silica fume. *Cement and concrete research*, *25*(8), 1615-1620.

Glass, G. K., Page, C. L., & Short, N. R. (1991). Factors affecting the corrosion rate of steel in carbonated mortars. *Corrosion Science*, 32(12), 1283-1294.

GSSI (2005). *GSSI handbook for RADAR inspection of concrete*. Retrieved from http://www.geophysical.com/Documentation/Manuals/MN72367D1%20Concrete%20Handbook.pdf

GSSI (2007). *RADAN 6.5 User's Manual.* GSSI

Jol, H. M. (Ed.). (2008). *Ground penetrating radar theory and applications*. Access Online via Elsevier.

Lahouar, S. (2003). *Development of data analysis algorithms for interpretation of ground penetrating radar data* (Doctoral dissertation, Virginia Polytechnic Institute and State University).

Lahouar, S., & Al-Qadi, I. L. (2008). Automatic detection of multiple pavement layers from GPR data. *NDT & E International*, 41(2), 69-81.

Loizos, A., & Plati, C. (2007). Accuracy of pavement thicknesses estimation using different ground penetrating radar analysis approaches. *NDT & E International*, 40(2), 147-157.

Maser, K. (1991). Bridge deck condition surveys using radar: case studies of 28 New England decks. *Transportation Research Record, (1304).*

Maser, K. R. (1994). Ground penetrating radar survey of pavement thickness on Mn/ROAD sections.

Maser, K. R. (1996). Condition assessment of transportation infrastructure using ground-penetrating radar. *Journal of infrastructure systems*, *2*(2), 94-101.

Minion, T., Barnes, C., Newhook, J. (2014). Through asphalt detection of concrete bridge deck deterioration using GRP. *CSCE Structural Conference Halifax, Nova Scotia.*

Moore, M., Phares, B. M., Graybeal, B., Rolander, D., & Washer, G. (2001).*Reliability of visual inspection for highway bridges, volume I: Final report* (No. FHWA-RD-01-020,).

Mortimer, R. G. (2000). *Physical Chemistry*. San Diego: Harcout/Academic Press.

Occupational Safety and Health Administration, Cincinnati Technical Center (May 20, 1990). "Electromagnetic Radiation and How It Affects Your Instruments. Near field vs. Far field." (Department of Labor – Public Domain content. Most of the content referenced by this work in this article is copied from a public domain document. In addition, this paper has provided references.). U.S. Dept of Labor. Retrieved 2010-05-09

Page, C. L., & Page, M. M. (Eds.). (2007). *Durability of concrete and cement composites*. Elsevier.

Redmond, E. (2007) The Use of Ground Penetrating Radar to Determine Corrosion Risk Potential for Steel Reinforced Exposed Concrete Bridge Decks. MASc thesis, Dalhousie University.

Roberts, R., (2014) personal communication April 2014.

Sbartaï, Z. M., Laurens, S., Balayssac, J. P., Arliguie, G., & Ballivy, G. (2006). Ability of the direct wave of radar ground-coupled antenna for NDT of concrete structures. *NDT & E International*, *39*(5), 400-407.

Sbartai, Z. M., Laurens, S., Rhazi, J., Balayssac, J. P., & Arliguie, G. (2007). Using radar direct wave for concrete condition assessment: Correlation with electrical resistivity. *Journal of applied geophysics*, *62*(4), 361-374.

Sketchley, A., Barnes, C., Newhook, J. (2014). Modeling reinforced concrete bridge decks as conductive media for GPR-based condition evaluation. *CSCE Structural Conference Halifax Nova Scotia.*

Schweitzer, P. A. (2009). Fundamentals of corrosion: mechanisms, causes, and preventative methods. CRC Press.

Silva, N. (2013). Chloride Induced Corrosion of Reinforcement Steel in Concrete-Threshold Values and Ion Distributions at the Concrete-Steel Interface. Chalmers University of Technology.

Sohanghpurwala, A. (2006). Manual on Service Life of Corrosion-Damaged Reinforced Concrete Bridge Superstructure Elements. TRB

Ulaby, F. T., Michielssen, E., & Ravaioli, U. (2001). Fundamentals of Applied Electromagnetics: XE-AU.... Prentice Hall.

Appendix A: Gain Correction

During data analysis it was noticed that the direct couple would have vastly different amplitude when held in the air when different configuration types were used. The first step was to run the GPR using different configuration types and ensure that the set gain was the same, in this case zero. From this quick qualitative test it was observed that the configuration type had an effect on the gain and was not recorded by the GPR. Due to the fact that the Chapter 7 tests were done using a custom configuration type and the field tests where done with what appears to be a concrete configuration type the effects of configuration type gain needed to be accounted for. This resulted in a more rigorous test setup. This test consisted of holding the antenna in the air, a concrete sample, a "dry" asphalt sample that had been soaked in salt water, and a "dry" asphalt sample. The asphalt samples were the same ones used in the Chapter 7 tests. The configuration types that were tested were custom with zero gain, concrete with zero gain and concrete with a gain of seven. Since their was no rebar in the sample the direct couple and reflection from the bottom plate were used to determine the gain. The gain was calculated using the Equation below.

$$Gain(dB) = 20\log\left(\frac{A_{concrete}}{A_{Custom}}\right)$$

Tables A 1 and A 2 summarise the result from the test. It should be noticed that the gain determined from the "air" sample difference significantly form the concrete and asphalt samples. The concrete and asphalt differ but the effects on the final result are relatively minor and at this point are not the deciding factor on accuracy. All data that appeared to have a concrete configuration type was automatically corrected for a 9.43 dB gain. If Radan indicated a gain of 5 dB's and if it appeared that a concrete configuration type was used, 14.43 dB's were removed from the data. If Radan indicated a gain of 7 dB's, 16.43 dB's were removed. The gain determined for the bottom was not used because it produced more erroneous results than the surface reflection. To get more accurate

result asphalt and concrete samples should be made with a metal plate inside the sample and the gain recalculated.

Surface Reflection				
Configuration Type\Sample	Air	Concrete	Salt	Asphalt
Custom	0.00	0.00	0.00	0.00
Concrete (zero gain)	10.33	9.59	9.43	9.43
Concrete (seven gain)	14.21	16.64	16.46	16.41

A 1: Gain caused by concrete configuration type for the surface reflection

Bottom Reflection			
Configuration Type\Sample	Concrete	Salt	Asphalt
Custom	0.00	0.00	0.00
Concrete (zero gain)	9.81	11.32	11.18
Concrete (seven gain)	16.84	13.41	13.32

A 2: Gain caused by concrete configuration type for bottom reflection